Monthly Notices
of the
ROYAL ASTRONOMICAL SOCIETY

MNRAS **432,** 3168–3185 (2013) doi:10.1093/mnras/stt672
Advance Access publication 2013 May 12

Towards a population synthesis model of objects formed by self-gravitating disc fragmentation and tidal downsizing

Duncan Forgan★ and Ken Rice

Scottish Universities Physics Alliance (SUPA), Institute for Astronomy, University of Edinburgh, Blackford Hill, Edinburgh EH9 3HJ, UK

Accepted 2013 April 17. Received 2013 April 16; in original form 2013 February 28

ABSTRACT

Recently, the gravitational instability (GI) model of giant planet and brown dwarf formation has been revisited and recast into what is often referred to as the 'tidal downsizing' hypothesis. The fragmentation of self-gravitating protostellar discs into gravitationally bound embryos – with masses of a few to tens of Jupiter masses, at semimajor axes above 30–40 au – is followed by a combination of grain sedimentation inside the embryo, radial migration towards the central star and tidal disruption of the embryo's upper layers. The properties of the resultant object depends sensitively on the time-scales upon which each process occurs. Therefore, GI followed by tidal downsizing can theoretically produce objects spanning a large mass range, from terrestrial planets to giant planets and brown dwarfs. Whether such objects can be formed in practice, and what proportions of the observed population they would represent, requires a more involved statistical analysis. We present a simple population synthesis model of star and planet formation via GI and tidal downsizing. We couple a semi-analytic model of protostellar disc evolution to analytic calculations of fragmentation, initial embryo mass, grain growth and sedimentation, embryo migration and tidal disruption. While there are key pieces of physics yet to be incorporated, it represents a first step towards a mature statistical model of GI and tidal downsizing as a mode of star and planet formation. We show results from four runs of the population synthesis model, varying the opacity law and the strength of migration, as well as investigating the effect of disc truncation during the fragmentation process. We find that a large fraction of disc fragments are completely destroyed by tidal disruption (typically 40 per cent of the initial population). The tidal downsizing process tends to prohibit low-mass embryos reaching small semimajor axis. The majority of surviving objects are brown dwarfs without solid cores of any kind. Around 40 per cent of surviving objects form solid cores of the order of 5–10 $M_\oplus$, and of this group a few do migrate to distances amenable to current exoplanet observations. Over a million disc fragments were simulated in this work, and only one resulted in the formation of a terrestrial planet (i.e. with a core mass of a few Earth masses and no gaseous envelope). These early results suggest that GI followed by tidal downsizing is not the principal mode of planet formation, but remains an excellent means of forming gas giant planets, brown dwarfs and low-mass stars at large semimajor axes.

Key words: accretion, accretion discs – methods: numerical – methods: statistical – planets and satellites: formation – stars: formation.

1 INTRODUCTION

Traditionally, there have been two distinct models or paradigms of planet formation in protostellar discs. In the core accretion (CA) paradigm (Pollack 1996; Hubickyj, Bodenheimer & Lissauer 2005), planetary mass bodies are assembled in a bottom-up process. The protostellar disc initially contains a population of interstellar grains of size ∼1 μm, which coagulate into larger particles. As the grains grow past a few cm in size, they settle to the mid-plane, aggregating into planetesimals a few km in size. The planetesimals can grow via collisions into solid protoplanetary cores, which can then accrete a thin gaseous envelope.

The fate of this solid core then depends on the mass it can reach – if the core exceeds a critical core mass of around 10 $M_\oplus$ (Mizuno 1980), the envelope accretion process is no longer thermally

★ E-mail: dhf@roe.ac.uk

regulated, resulting in runaway growth of the atmosphere, producing gas and ice giants. Below this critical core mass, the gas accretion remains slow, and terrestrial planets can be formed.

CA is certainly the most accepted model of planet formation, and it is the most successful at explaining the majority of the observed exoplanet population. Despite this, predictions of deserts in the exoplanet distribution at short periods and low mass have not been borne out by observations, and the existence of highly compact systems such as Kepler-11 (Lissauer et al. 2011) are not easily explained.

Questions also remain regarding certain stages of the core growth process. There are barriers to grain growth at various size scales. The most famous is the 'metre barrier', which is in reality a mixture of inhibiting factors that take effect for grain sizes as small as millimetres depending on the local disc properties. As grains increase in size, their relative velocities increase, and the probability of continued growth decreases (Blum & Wurm 2008). Also, gas drag works most efficiently on metre-sized bodies, causing rapid radial drift and loss of solid material on to the central star (Whipple 1973; Weidenschilling 1977). More recently, light has been shed on the 'bouncing barrier', which occurs at slightly lower relative velocities, and also inhibits grain growth (Güttler et al. 2010; Windmark et al. 2012).

Conversely, in the gravitational instability (GI) paradigm (Cameron 1978; Boss 1997), planetary-mass objects are assembled in a top-down fashion through fragmentation of the gaseous protostellar disc. This occurs during a relatively brief phase of the disc's life where it is sufficiently massive to be self-gravitating, and can become gravitationally unstable. Gravitationally unstable discs must satisfy the Toomre criterion (Toomre 1964):

$$Q = \frac{c_s \kappa_e}{\pi G \Sigma} < 1.5\text{–}1.7, \tag{1}$$

where Q is the Toomre parameter, c_s is the local sound speed of the gas, κ_e is the local epicyclic frequency (equal to the angular velocity Ω in Keplerian discs) and Σ is the disc surface density. This is a linear stability criterion, and for axisymmetric perturbations $Q < 1$ for instability. Equation (1) refers to non-axisymmetric perturbations, where the critical Q value has been established by simulations (see e.g. Durisen et al. 2007 for a review).

The onset of GI produces trailing spiral density waves which heat the disc, increasing Q. The density perturbations produced by the spiral waves eventually decay, allowing the disc to cool and become unstable once more. As new spiral structure is generated by the instability, this cycle of growth and decay introduces turbulence into the gas, usually referred to as gravitoturbulence (Gammie 2001). If the disc's angular momentum transport is locally determined, this turbulence can be represented by a 'pseudo-viscosity' ν (Balbus & Papaloizou 1999; Lodato & Rice 2004; Forgan et al. 2011), and as such is amenable to the Shakura & Sunyaev (1973) α-parametrization:

$$\nu = \alpha c_s H, \tag{2}$$

where H is the disc scale-height. This description greatly simplifies the disc evolution to a viscous form (although typically non-linear and only soluble numerically) such that, if we assume that the disc is axisymmetric, then the surface density $\Sigma(r, t)$ evolves according to (Lynden-Bell & Pringle 1974; Pringle 1981)

$$\frac{\partial \Sigma}{\partial t} = \frac{3}{r}\frac{\partial}{\partial r}\left[r^{1/2}\frac{\partial}{\partial r}\left(\nu \Sigma r^{1/2}\right)\right] - \dot{\Sigma}_{\rm wind}, \tag{3}$$

where $\dot{\Sigma}_{\rm wind}$ represents mass-loss from the disc due to a disc wind. The disc can respond to the heating caused by the instability via radiative cooling, reducing the local sound speed and decreasing Q. As self-gravitating discs will only exist in the early stages of star formation, we should also expect a mass loading term in these equations which can have significant consequences for the disc's evolution (see e.g. Clarke 2009).

As a result of the competition between heating and cooling, gravitationally unstable discs can maintain what is referred to as a marginally unstable state (Paczynski 1978), where the shock heating and radiative cooling become balanced, Q maintains a self-regulated value around the critical value, and the disc becomes quasi-steady. If the disc is marginally unstable and in local thermodynamic equilibrium, then we can solve for α (Gammie 2001):

$$\alpha = \frac{4}{9\gamma(\gamma - 1)\beta_c}, \tag{4}$$

where we have defined β_c as a dimensionless expression of the local cooling time $t_{\rm cool}$:

$$\beta_c = t_{\rm cool}\Omega. \tag{5}$$

For a self-gravitating disc to fragment, this self-regulating mechanism must be broken. The density perturbations induced by the GI have the behaviour (Cossins, Lodato & Clarke 2009; Rice et al. 2011):

$$\left\langle \frac{\Delta \Sigma_{\rm rms}}{\Sigma} \right\rangle \propto \frac{1}{\sqrt{\beta_c}} \propto \sqrt{\alpha}. \tag{6}$$

Therefore, to produce a density perturbation of sufficiently high amplitude that it can collapse into a bound object, the local cooling time must be sufficiently short, or equivalently the local gravitational stresses must be sufficiently high.

It is reasonably clear that self-gravitating stresses saturate at some value of α, setting a lower limit for the cooling time, below which a marginally unstable state can no longer be maintained. Below this critical cooling time $\beta_{\rm crit}$, the disc is no longer able to achieve thermodynamic balance, and fragmentation is expected to occur. The critical cooling time is a function of the ratio of specific heats (γ), but the saturating value of α is fixed at around 0.06 (Gammie 2001; Rice, Lodato & Armitage 2005).

The precise saturating value of α is currently unclear due to convergence issues (Meru & Bate 2011). Indeed, it may be the case that fragmentation proceeds in a stochastic fashion, where the power spectrum of density fluctuations is such that a weak perturbation results in fragmentation, and the traditional fragmentation criteria do not delineate fragmenting/non-fragmenting configurations, but indicate where the probability of fragmentation is close to unity. If this is the case, it may be that fragmentation can occur with low probability at values of β_c as high as 20–50 (Paardekooper 2012; Hopkins & Christiansen 2013). This debate is yet to be fully resolved, but there are indications that careful consideration of the effects of artificial viscosity (Lodato & Clarke 2011) and a more appropriate implementation of radiative cooling (Rice, Forgan & Armitage 2012) can help to address this problem, and that the saturating value of α remains of the order of 0.1. As yet, true stochastic fragmentation has not been observed in global disc simulations. Due to our current ignorance of how its properties may be incorporated into this work, we will not include it in this analysis.

Regardless, these arguments have to some extent excluded the effects of mass infall, thermal history (Clarke, Harper-Clark & Lodato 2007) and stellar irradiation (Kratter & Murray-Clay 2011). Later work has generalized this fragmentation criterion in terms of critical

scales such as the Jeans mass (Forgan & Rice 2011, 2013) or the Hill radius (Rogers & Wadsley 2012), which agree well with results derived from direct investigation from the spiral structure (Boley et al. 2010).

Requiring the Q-condition for GI and a second criterion for fragmentation restricts the disc radii at which fragments may form. Typically, the inner disc does not cool efficiently enough to maintain low enough Q values, and is therefore stable against self-gravity. Also, gravitational stresses tend to decrease with increasing proximity to the central star (Armitage, Livio & Pringle 2001; Clarke 2009; Rice & Armitage 2009; Rice, Mayo & Armitage 2010).

Fragmentation is therefore consigned to the outer disc, and typically to radii above 30 or 40 au (Rafikov 2005; Matzner & Levin 2005; Boley et al. 2006; Whitworth & Stamatellos 2006; Stamatellos & Whitworth 2008; Clarke 2009; Forgan et al. 2009; Kratter, Murray-Clay & Youdin 2010; Vorobyov & Basu 2010; Forgan & Rice 2011). Estimates for the fragment mass tend to place a lower limit of 3–5 $M_{\rm Jup}$ (Kratter et al. 2010; Forgan & Rice 2011). These two results alone would appear to be enough to discount the GI theory as a means of forming lower mass planets at disc radii inside 30 au. Equally, CA has difficulty explaining the existence of massive planets with semimajor axes above 30 au, and so it may be the case that planet formation proceeds via both CA and GI (Boley 2009).

However, the recent reformulation of the GI theory into what is commonly referred to as 'tidal downsizing' (Boley et al. 2010; Nayakshin 2010a,b, 2011b; Boley, Helled & Payne 2011) has revived the possibility that the GI formation mode could produce low-mass planets at low semimajor axis. The key to this revival is the study of the subsequent evolution of the disc fragments into planetary embryos. Three key physical processes shape the fate of the embryo:

(i) *Dust growth and sedimentation*. As grains grow inside the embryo, the sedimentation velocity of the grains increases, drawing them towards the pressure maximum at the embryo's centre. If this process is efficient, the gravitational field at the centre of the embryo will become dominated by solids. The solids can become self-gravitating, potentially even gravitationally bound, forming a solid core. As the temperature at the centre of the embryo increases, the grains can eventually be vaporized, ending the growth of the core.

(ii) *Radial migration*. Differential torques induced by the disc on the embryo can result in inward radial migration, in much the same way as protoplanets in the CA paradigm.

(iii) *Tidal disruption*. As an embryo migrates inwards, its physical radius will be comparable to the Hill radius. As this occurs, the upper layers will become unbound, and hence stripped from the embryo.

By comparing the time-scales on which these three processes occur, Nayakshin (2010a) gives several possible outcomes for the embryo. In some cases, it is conceivable that a solid core of less than 10 $M_\oplus$ can be formed inside the embryo, which has its upper layers completely disrupted, leaving a terrestrial protoplanet. Equally, inefficient core formation and strong tidal disruption could result in the entire embryo being destroyed and accreted by the star, giving rise to outburst behaviour (e.g. Vorobyov & Basu 2005; Boley et al. 2010; Dunham & Vorobyov 2012; Nayakshin & Lodato 2012). Intermediate cases produce giant planets both with and without cores depending on the sedimentation time-scale. If the core is not fully gravitationally bound before the embryo is disrupted, then this could potentially produce belts of planetesimals (Nayakshin & Cha 2012), or generally deliver processed solid material that can affect the overall disc chemistry (Boley et al. 2010, 2011).

This production of planets of varying types and masses, which circumvents the need for planetesimal growth without precluding the existence of asteroid belts, makes the tidal downsizing hypothesis an attractive one for planet formation theorists. However, it remains unclear what distribution of object mass and semimajor axis should be expected from self-gravitating disc fragmentation. A common criticism of GI theories as a whole is the lack of population synthesis models, which have been implemented for the CA model with a great deal of success (e.g. Ida & Lin 2004, 2008; Alibert et al. 2005; Mordasini et al. 2012).

In this paper, we wish to remedy this by presenting a simple population synthesis model for disc fragmentation followed by tidal downsizing. This model is still missing some physical processes, and simplifies others, but it gives the broad strokes of what stellar and planetary systems we can expect to see produced by this theory. As such, we present it as the first stage in a continuing series of work (much as was done with the population synthesis models of CA). We couple the equations of Nayakshin (2010a,b, 2011b) with semi-analytic models of disc evolution incorporating X-Ray photoevaporation (Rice & Armitage 2009; Owen, Ercolano & Clarke 2011), and evolve a large ensemble of planetary embryos formed in a variety of self-gravitating protostellar discs. While uncertainties remain about the underlying distributions of disc mass and radius at early times, a uniform sampling of these parameters allows us to explore the exoplanet parameter space in which we can expect the GI formation mode to leave its signature. This will allow the statistical properties of the two principal planet formation theories, CA and GI, to be compared much more directly than has been possible until now.

The paper is structured as follows: in Section 2, we discuss the implementation of the equations that describe the sedimentation, migration and disruption of embryos, as well as the disc models used in this work. In Section 3, we display the resulting statistical distributions as a function of a few remaining free parameters. In Section 4, we discuss the implications of these models for the tidal downsizing hypothesis, critically assess the current weaknesses of our approach and advocate avenues for further work. Finally, in Section 5, we summarize the work.

2 METHOD

2.1 A simple semi-analytic model of tidal downsizing

In this section, we summarize the equations governing embryo formation, core formation and the subsequent migration/disruption processes that can occur. Throughout, we rely heavily on the equations given by Nayakshin in his three papers outlining the tidal downsizing hypothesis (Nayakshin 2010a,b, 2011b). We also use semi-analytic disc models as described in Rice & Armitage (2009), and determine fragmentation and fragment masses using the Jeans mass formalism as described in Forgan & Rice (2011).

2.1.1 Conditions for disc fragmentation

To first assess where fragmentation can occur, we calculate the Toomre Q criterion at all disc radii, as well as the Γ_J criterion outlined in Forgan & Rice (2011), where

$$\Gamma_J = \frac{M_J}{\dot{M}_J}\Omega, \tag{7}$$

and M_J is the local Jeans mass inside a spiral perturbation. This condition allows us to determine at what rate the Jeans mass is changing. Regimes where the Jeans mass is decreasing rapidly will be prone to fragmentation. If we assume that the disc is marginally unstable and in a steady state, then

$$\Gamma_J = \left(3/2\left(-\frac{1}{\beta_c} + \frac{9\alpha\gamma(\gamma-1)}{4}\right)\right)^{-1}. \quad (8)$$

If the disc is in thermal equilibrium, then $\Gamma_J \to \infty$, and the disc will not fragment. If β_c is sufficiently low that thermal equilibrium would demand that α would exceed the value $\alpha_{\rm sat}$ at which gravito-turbulent transport is expected to saturate, i.e. $\alpha > \alpha_{\rm sat} \sim 0.1$, we set $\alpha = \alpha_{\rm sat}$ and Γ_J becomes negative. As β_c decreases, Γ_J remains negative, and its magnitude decreases. Once Γ_J is sufficiently small and negative, we can see that the local Jeans mass is decreasing sufficiently quickly that a local spiral density perturbation will soon exceed the Jeans mass, and begin the fragmentation process.

We therefore demand that (in disc regions where $Q \leq 1.5$) the local Jeans mass must be decreasing at a rate such that

$$-5 < \Gamma_J < 0 \quad (9)$$

for fragmentation to occur. The exact critical values for Γ_J are currently unclear, but the above produce results consistent with conventional cooling time criteria (Forgan & Rice 2011, 2013). The value of Γ_J sets a time-scale for fragmentation rather than specifying whether or not it will occur. If $\Gamma_J < -5$, then in theory fragmentation remains possible, but unlikely, as disc evolution will typically act to prevent this.

The advantage of using the Jeans mass criterion is that it immediately identifies an initial fragment mass M. From Forgan & Rice (2011), this is

$$M = M_J = \frac{4\sqrt{2}\pi^3}{3G}\frac{Q^{1/2}c_{\rm s}^2 H}{\left(1+\frac{\Delta\Sigma}{\Sigma}\right)}. \quad (10)$$

While disc fragmentation is an inherently three-dimensional process, the initial conditions provided by the disc are roughly two dimensional. If the surface density perturbation induced by a spiral density wave $\Delta\Sigma/\Sigma$ is of the order of unity, the perturbations will become non-linear, and fragmentation can be expected to occur (this statement is true despite the current debate regarding stochastic fragmentation). In other words, at the point of fragmentation, a 2D measure is sufficient to identify when fragmentation occurs, but the details of the fragment's subsequent evolution are 3D. As the discs we use in the modelling done here are axisymmetric, surface density is in fact a 1D measure, and for these purposes is sufficient to control/govern the fragmentation process. As with much semi-analytic modelling, using 1D measures as is done here is a necessary and appropriate sacrifice for the sake of computational expediency.

Using the empirical relation for $\Delta\Sigma/\Sigma$ derived by Rice et al. (2011), we can give the following form for M:

$$M = \frac{4\sqrt{2}\pi^3}{3G}\frac{Q^{1/2}c_{\rm s}^2 H}{\left(1+4.47\sqrt{\alpha}\right)}. \quad (11)$$

Fragments are formed wherever both the Q and Jeans mass criteria specified above are satisfied. We might expect fragments to form at spacings of approximately 2 Hill radii, so that feeding zones do not strongly overlap (Lissauer 1987). To reflect our current uncertainty in this matter, the precise value of the spacing is uniformly distributed between 1.5 and 3 Hill radii. This also allows us to probe a larger variety of initial fragment properties from what is a limited set of initial disc models.

This is sufficient to create the initial embryo population. We must now investigate the evolution of the embryos individually.

2.1.2 *Initial properties of the fragment/embryo*

By appealing to the analogy of the opacity limit for fragmentation in star formation (Low & Lynden-Bell 1976; Rees 1976), it can be seen that fragments are initially akin to the 'first cores' (FCs) of the star formation process (e.g. Masunaga, Miyama & Inutsuka 1998). We will refer to these as FCs to avoid confusion with the later solid cores that may develop inside these embryos.

If these fragments are indeed FCs, it is appropriate to model them as polytropic spheres. The properties of the polytrope depend on the initial temperature (taken usually to be $\sim$10 K) and the critical density $\rho_{\rm ad}$ at which the gas switches between isothermal and adiabatic behaviour. These quantities constrain the initial radius of the FC (Masunaga et al. 1998; Masunaga & Inutsuka 1999). If we follow the route of Nayakshin (2010a) and define the opacity law

$$\kappa(T) = \kappa_0\left(\frac{T}{10\,{\rm K}}\right)^{p_\kappa}, \quad (12)$$

and the following scaled quantities:

$$m_1 = \frac{M}{0.01\,{\rm M}_\odot}$$

$$T_1 = \frac{T}{10\,{\rm K}}$$

$$\kappa_* = \frac{\kappa_0}{0.01}, \quad (13)$$

we find the FC radius R as (see Nayakshin 2010a for more)

$$R = 17.5\,{\rm au}\, m_1^{-1/3} T_1^{(1+4p_\kappa)/9}\kappa_*^{4/9}. \quad (14)$$

The temperature of the FC will be close to the virial temperature:

$$T_{\rm vir} = \frac{GM\mu}{3k_B R} = 146\,{\rm K}\, m_1^{4/3} T_1^{-(1+4p_\kappa)/9}\kappa_*^{-4/9}. \quad (15)$$

The luminosity of the FC is a non-trivial function of the opacity power-law index p_κ, and becomes somewhat cumbersome to write down in general terms. Hence, Nayakshin evaluates expressions for $p_\kappa = 1$, 2, and as such gives the equivalent expressions for the cooling time for both opacity laws, assuming the binding energy of a sphere:

$$t_{\rm cool,0} = 380\,{\rm yr}\, m_1^{2/3} T_1^{-4/3}\kappa_*^{1/9} \quad (16)$$

$$t_{\rm cool,0} = 5700\,{\rm yr}\, m_1^{2} T_1^{-19/9}\kappa_*^{-1/3}. \quad (17)$$

The '0' in the subscript indicates that these are initial values for the cooling time. Nayakshin shows that as the FC contracts, the cooling time increases:

$$t_{\rm cool}(t) = t_{\rm cool,0} + (1+p_\kappa)\,t. \quad (18)$$

As a result, the temperature evolves according to

$$T(t) = T(0)\left[1+(1+p_\kappa)\frac{t}{t_{\rm cool,0}}\right]^{\frac{1}{1+p_\kappa}}. \quad (19)$$

The evolution of the temperature will be crucial to the survival of grains inside the embryo, as will be discussed in the next section. Finally, we can express the contraction of the embryo as

$$R(t) = \frac{R(0)}{\left[1+2\frac{t}{t_{\rm cool,0}}\right]^{1/2}}. \quad (20)$$

These analytic expressions should be contrasted with the more detailed calculations made by Helled, Podolak & Kovetz (2006) and subsequent works (Helled & Schubert 2008; Helled, Podolak & Kovetz 2008) which numerically integrate the equations of stellar evolution, with a spherically symmetric embryo as initial conditions. Fig. 1 of Nayakshin (2010b) shows typical temperature evolution tracks using the above equations for FCs between 3 and 30 $M_{\rm Jup}$, and these compare well with the temperature evolution shown in fig. 2 of Helled et al. (2006). However, we should note that the contraction time-scales shown here are much longer than those given by calculations where the opacity is allowed to vary due to grain evolution (Helled & Bodenheimer 2011), and this has important implications for future work (see Section 4).

2.1.3 Grain growth and sedimentation

If there has not been significant grain growth or enrichment before disc fragmentation, the protostellar disc grains (of no more than a few microns in size) will be extremely slow to sediment to the centre of the embryo. Therefore, an initial phase of grain growth must be completed before the embryo can form a core on a reasonable time-scale. This grain growth time-scale $t_{\rm gr}$ is initially defined by the Brownian motion of the grains (Dullemond & Dominik 2005), but quickly becomes dominated by differential settling, where (at relatively small grain sizes) the larger grains experience greater sedimentation velocity.

Initially, the grains are small enough for their motion to be tightly coupled to that of the gas. The grain growth process is physically very similar to that of the CA paradigm, with an added gravitational acceleration towards the embryo's centre, which for a constant density embryo is

$$a_{\rm gr}(r) = -4/3\pi G\rho r, \tag{21}$$

where $r = [0, R]$ is the grain's radial position. The drag force due to the embryo's gas can be expressed as a combination of Stokes and Epstein regimes (Weidenschilling 1977; Boss 1998; Nayakshin 2010a):

$$\frac{{\rm d}v_s}{{\rm d}t} = -\frac{\rho c_{\rm s}}{\Sigma_s}\frac{\lambda}{\lambda + s}(v_s - v) - 4/3\pi G\rho r, \tag{22}$$

where λ is the mean free path of the grain, s is the grain size, and v_s and v are the velocities of the grains and gas, respectively. We have defined $\Sigma_s = \rho_{\rm bulk} s$, where the bulk density of the grains $\rho_{\rm bulk} \approx 1\,{\rm g\,cm^{-3}}$. Grains will quickly reach a terminal velocity $v_{\rm sed}$, which can be found by solving for ${\rm d}v_s/{\rm d}t = 0$,

$$v_{\rm sed} = \frac{-4\pi G\Sigma_s R}{3c_{\rm s}}\frac{\lambda + s}{\lambda}. \tag{23}$$

Differential sedimentation allows the larger grains to sweep up the smaller grains, and results in a mass growth rate:

$$\frac{{\rm d}m}{{\rm d}t} = \pi s^2 f_{\rm g}\rho v_{\rm sed}, \tag{24}$$

where s is the grain size, $f_{\rm g}$ is the mass fraction in grains and ρ is the local gas density (i.e. in this initially well-mixed phase, the volume density of grains $\rho_{\rm g} = f_{\rm g}\rho$). Converting this into a growth rate for s gives

$$\frac{{\rm d}s}{{\rm d}t} = \frac{f_{\rm g}\rho}{4\rho_s}v_{\rm sed}, \tag{25}$$

and so we can define a grain growth e-folding time-scale:

$$t_e = \frac{s}{\frac{{\rm d}s}{{\rm d}t}} = \frac{3c_{\rm s}}{\pi f_{\rm g}\rho G R}. \tag{26}$$

Given an initial grain size (s_0) and final grain size ($s_{\rm crit}$) before sedimentation can become significant, then the growth time-scale is

$$t_{\rm gr} = \frac{3c_{\rm s}}{\pi f_{\rm g}\rho G R}\ln\left(\frac{s_{\rm crit}}{s_0}\right). \tag{27}$$

Once the grains have grown to $s_{\rm crit}$, the entire body of grains (which we refer to as the 'grain sphere') will begin to sediment, quickly accelerating to critical velocity. As the sedimentation velocity is a function of R, the sedimentation time is independent of radius, i.e. all shells of sedimenting dust will reach the centre of the embryo at the same time (if the embryo is uniform). The sedimentation time is

$$t_{\rm sed} = \frac{R}{v_{\rm sed}} = \frac{3c_{\rm s}}{4\pi G\Sigma_s}\frac{\lambda}{\lambda + s}. \tag{28}$$

The sedimentation of grains can be limited by destructive collisions (Blum & Wurm 2008). At velocities of several metres per second, collisions will result in fragmentation rather than growth. This limits the maximum value of $v_{\rm sed}$, and as such the sedimentation time-scale has a lower limit (Nayakshin 2010b). Generally speaking, these equations show similar dependences on temperature and dust-to-gas ratio as those of Helled's calculations (see e.g. appendix 1 of Helled & Bodenheimer 2011), but we note that the physics we employ here is much simpler.

In particular, note that our equations describe the bulk motion of the grains, and do not incorporate the changing radial profile or temperature of the embryo. The evolution of the clump's photosphere will have consequences that these equations cannot yet model. Radiative heating of the embryo can have significant consequences for grain settling and destruction (Helled et al. 2008; Helled & Bodenheimer 2011).

2.1.4 Turbulence as a suppressor of settling

How should we select $s_{\rm crit}$ in equation (27)? We have neglected turbulence in this analysis, which will act to prevent gravitational settling (Fromang & Papaloizou 2006). We can approximate the effects of turbulent mixing using a 1D diffusion equation in spherical geometry, with the diffusion coefficient selected using the Shakura & Sunyaev (1973) viscosity prescription:

$$D = \alpha c_{\rm s} R. \tag{29}$$

If the gas is initially a constant density sphere, the dust sphere settles to an equilibrium solution

$$\rho_{\rm s} = \rho_{\rm s,0}\exp\left[-\frac{R^2}{H_d^2}\right], \tag{30}$$

where

$$H_d = \sqrt{2Dt_{\rm sed}}. \tag{31}$$

If we re-express this as an aspect ratio:

$$\frac{H_d}{R} = \left[\frac{3\alpha}{2}\frac{\Sigma}{\Sigma_s}\frac{\lambda}{\lambda + s}\right]^{1/2}. \tag{32}$$

For gravitational settling to dominate over the turbulent mixing the above aspect ratio should be much less than 1. For a given turbulence parameter α, we can assume that $s_{\rm crit}$ is found by setting $H_d/R = 1$ and solving for s. Unlike the detailed calculations of Helled et al. (2008) and Helled & Bodenheimer (2011), convection is not considered here. They find that embryos are likely to be highly convective initially, and this has important consequences for

slowing the settling process, and returning settled grains back to the upper envelope. It is therefore crucial that future models incorporate convection (see Section 4 for more).

2.1.5 The effect of the contracting embryo

The grain growth time-scale in equation (27) tacitly assumes a static embryo. However, the grain growth time-scale is sufficiently long compared to the cooling time that we should expect the embryo to cool and contract significantly during this time. This compression should accelerate grain growth. The growth time-scale scales as

$$t_{\rm gr} \propto \frac{c_{\rm s}}{\rho R} \propto \left(\frac{T(t)}{T(0)}\right)^{-3/2}. \tag{33}$$

Altering the size growth equation as follows:

$$\frac{{\rm d}s}{{\rm d}t} = \left(\frac{{\rm d}s}{{\rm d}t}\right)_0 \left[1 + (1+p_\kappa)\frac{t}{t_{\rm cool,0}}\right]^{1.5/(1+p_\kappa)}. \tag{34}$$

Integrating this gives the more accurate estimate of the growth time-scale:

$$t_{\rm gr} = \frac{t_{\rm cool,0}}{1+p_\kappa}\left[\left(1 + \frac{2.5+p_\kappa}{t_{\rm cool,0}} t_{\rm gr,0}\right)^{\xi} - 1\right], \tag{35}$$

where $\xi = (1 + p_\kappa)/(2.5 + p_\kappa)$. This revised growth time-scale can be over an order of magnitude shorter than the static estimate, $t_{\rm gr,\,0}$. Indeed, numerical experiments indicate that the true time-scale can be another factor of 2 shorter still (Nayakshin 2010a), and as mentioned already, these time-scales can be orders of magnitude shorter when opacity evolution due to grain growth is included (Helled & Bodenheimer 2011).

2.1.6 Core formation

The total mass in solids is

$$M_{\rm s} = f_{\rm g} M, \tag{36}$$

where $f_{\rm g} = 0.02$ for solar metallicity. For an embryo of $1\,M_{\rm Jup}$, this gives a fiducial maximum core mass of around $60\,{\rm M}_\oplus$. Approximately two-thirds of the solids mass is ices (Nayakshin 2010b), so melting can reduce this maximum mass by the same factor.

As the sedimentation time-scale is independent of radius, the grain sphere, initially of radius $R_{\rm g}(0)$ (which is equal to the radius of the FC), will begin contracting according to

$$R_{\rm g}(t) = R \exp\left[-\frac{t}{t_{\rm sed}}\right]. \tag{37}$$

This allows us to identify the time-scale $t_{\rm self}$ on which the density of grains exceeds the local gas density, and the grains become self-gravitating. This time-scale is

$$t_{\rm self} = t_{\rm sed}\frac{\ln f_{\rm g}^{-1}}{3}. \tag{38}$$

The factor of 3 emerges from assuming a spherically symmetric geometry. Once the dust sphere is self-gravitating, the sedimentation velocity is modified so that the gravitational acceleration comes only from mass inside the dust sphere:

$$v_{\rm sed} = -\frac{GM_{\rm s}(R_{\rm s})}{R^2}\frac{\Sigma_s}{\rho c_{\rm s}}\frac{\lambda + s}{\lambda}. \tag{39}$$

The mass interior to the dust sphere remains constant, and therefore the differential equation for $R_{\rm s}$ takes the form

$$\frac{{\rm d}R_{\rm s}}{{\rm d}t} = -\frac{A}{R_{\rm s}^2}, \tag{40}$$

where A is some constant, and has the solution

$$R(t) = R(t_{\rm self})\left[1 - 3\frac{t - t_{\rm self}}{t_{\rm sed}}\right]^{1/3}. \tag{41}$$

The contraction remains homologous, but is more rapid than the non-self-gravitating stage. The free-fall time of the dust sphere, i.e. the time required for all grains to collapse to infinite densities, becomes approximately twice the sedimentation time-scale (Nayakshin 2010b).

In this self-gravitating phase, the grain sphere can still be dissipated. If, for example, the outer envelope of gas is removed, the resulting pressure gradient in the grain–gas mix can destroy the grain sphere. This is in part because the grain sphere is self-gravitating, but not gravitationally self-bound. If the grain sphere can contract sufficiently to become self-bound, then even the dissipation of the outer envelope will not unbind the sphere. Nayakshin (2011b) refers to this stage as the 'grain cluster' stage, as an analogy to star clusters which survive interstellar gas dispersal.

If the grain sphere's self-gravity dominates over the local gas pressure gradient, then the grain sphere can enter the grain cluster phase. This is in essence a Jeans length argument, and the usual calculations apply. The pressure gradient is of the order of

$$\frac{{\rm d}P}{{\rm d}R} \sim \frac{\rho k_B T}{\mu m_H R}, \tag{42}$$

and should be equal to the gravitational force per unit volume for hydrostatic equilibrium:

$$f_{\rm grav} \sim \frac{GM_{\rm enc}(R)}{R^2}(\rho + \rho_s). \tag{43}$$

Equating these (and assuming $\rho \ll \rho_{\rm g}$) gives the Jeans length as

$$\lambda_J = \left[\frac{3}{4\pi G}\frac{k_B T}{\mu m_H}\frac{\rho}{\rho_s^2}\right]^{1/2}. \tag{44}$$

Once the grain sphere radius contracts below this length, then the final process of core formation can begin, which is presumed to be rapid (Boss 1998; Nayakshin 2011b), although the process requires further study to ascertain this (see Section 4).

2.1.7 Ice melting, grain vaporization and hydrogen dissociation

A fundamental barrier to solid core formation is the increasing temperature of the embryo. As the embryo contracts, the central temperature increases, and the chemistry and phase of the grains will change. At temperatures above ∼200 K, the ice mantles of the grains will melt, preventing volatiles from becoming part of the core. At temperatures above 1400 K, the grains can be vaporized, preventing a solid core from forming at all. Embryos of relatively large initial mass will have higher initial temperatures, and as a result will be more likely to vaporize their grains before a core can form.

At temperatures above 2000 K, the molecular hydrogen inside the embryo begins to dissociate. The energy that must be stored in internal degrees of freedom to achieve this depletes the embryo's pressure support, allowing it to begin a second collapse. In star formation, this precipitates the formation of the 'second core' (Masunaga et al. 1998), the bound entity which is the protostar

itself. Once this has occurred, the FC equations no longer apply, and the embryo has attained a new quasi-static configuration with a greatly reduced physical radius.

When objects reach this stage, we switch to the mass–radius model of Burrows et al. (1997) (see e.g. Burrows, Heng & Nampaisarn 2011). We deem any object which reaches this stage with a total mass greater than $13 M_{\rm Jup}$ to be a 'brown dwarf'. Objects which reach this stage and have a mass less than $13\,M_{\rm Jup}$ are split into several categories depending on their final configuration. Objects which have managed to form a core before melting are recorded as 'icy core' objects; objects which form a core after melting are recorded as 'rocky core' objects and objects which do not form a solid core before the grains vaporize are simply labelled 'no core' objects.

From equation (15), $T \propto M^{2/3}$, which gives a lower mass limit for objects which are able to undergo H_2 dissociation before being tidally disrupted.

2.1.8 Disc migration

While the embryo is evolving internally, the disc is evolving externally, and differential torques will result in planetary migration. The current wealth of the literature on planetary migration (see Kley & Nelson 2012; Baruteau & Masset 2013 for reviews) is predicated on planets represented either as points or as uniform density spheres. The 'FC' calculations shown above negate both assumptions, as the embryo radius will typically exceed the Hill radius, and as such more sophisticated hydrodynamic simulations are required to show the migration of disc fragments in a disc which may still be self-gravitating (e.g. Baruteau, Meru & Paardekooper 2011; Cha & Nayakshin 2011; Michael, Durisen & Boley 2011; Boss 2013). These simulations have shown that the migration of clumps in self-gravitating discs is non-trivial, and typically much more rapid than calculations based on non-self-gravitating discs would predict. Also, the migration direction becomes a function of the disc's viscosity, as has been found in other migration simulations (cf. Bitsch, Boley & Kley 2013).

This being said, it is useful to use the standard migration time-scale calculations (as was done by Nayakshin 2010a) to allow comparison with their work, as well as to keep the complexity of the semi-analytic model under control. Indeed, it is as yet unclear if a full semi-analytic description of fragment migration has emerged from numerical simulations, and will most likely require further study of the parameter space before they can be formulated.

From Bate, Bonnell & Bromm (2003), the migration regime depends on the embryo mass. Type I migration occurs if $M \leq M_{\rm t}$, and type II if $M > M_{\rm t}$, where the transition mass

$$M_{\rm t} = 2M_* \left(\frac{H}{R}\right)^3. \tag{45}$$

For type I migration, the migration time-scale is

$$t_{\rm I}(a) = \left(\frac{M}{M_*}\Omega\right)^{-1} \frac{H}{a}, \tag{46}$$

and for type II

$$t_{\rm II}(a) = \frac{1}{\alpha\Omega}\left(\frac{H}{a}\right)^{-2} \tag{47}$$

(where we have assumed a self-gravitating, $Q = 1$ disc). As expected, type I migration is typically several orders of magnitude faster than type II.

Planet–disc interactions do more than modify the planet's semi-major axis. Other orbital elements can also be modified, principally the eccentricity and inclination. Co-orbital Lindblad resonances will typically act to dampen eccentricities if the planet is fully embedded (Artymowicz 1993), but if the planet opens a gap dampening is suppressed, and can even result in eccentricity growth depending on the strength and saturation of corotation resonances (Ogilvie & Lubow 2003; Moorhead & Adams 2008). In the case of massive planets (i.e. above $1\,M_{\rm Jup}$), simulations indicate that eccentricity is generally damped (Bitsch & Kley 2010; Kley & Nelson 2012), but a multi-embryo environment may produce larger eccentricities through clump–clump scattering, or even eject them from the system entirely (Boley et al. 2010; Stamatellos 2013). We assume that the embryos adopt coplanar, circular orbits for simplicity.

2.1.9 Tidal disruption

If the embryo's radius exceeds its Hill radius

$$R_H = a\left(\frac{M}{3M_*}\right)^{1/3}, \tag{48}$$

the upper layers can become unbound. As the semimajor axis decreases, the radial acceleration will typically increase, while the embryo contraction rate decreases with time. The inevitable result is tidal disruption. Appendix A of Nayakshin (2011b) indicates that, while irradiation of the upper envelope by the star can also achieve disruption, tidal disruption tends to occur first for embryos around low-mass stars (although the modification of the disc structure due to the radiation field, not modelled in this work, can affect the migration process, cf. Fouchet et al. 2012).

The fate of the solid material inside the embryo depends on the evolutionary stage. As previously mentioned, if the grain sphere is not self-bound, then it will become unbound as the envelope disappears. If the embryo is completely dissolved, the resulting solids, which may have grown significantly since the embryo's birth, are dispersed into the protoplanetary disc, as processed solids and rubble piles (Boley et al. 2010, 2011), potentially even planetesimals (Nayakshin & Cha 2012).

If the grain sphere has become self-bound and initiated its final collapse, then the stripping of the envelope can allow the emergence of a terrestrial mass protoplanetary core.

2.2 Evolution of the protostellar disc

We assume that the disc is axisymmetric and that the surface density, $\Sigma(r, t)$, evolves viscously according to equation (3). In a steady state, this can be integrated to give an expression for the mass accretion rate, $\dot{M}$, which, at radii large compared to the radius of the star, is (Pringle 1981)

$$\dot{M} = 3\pi\nu\Sigma. \tag{49}$$

One of the main uncertainties in disc evolution is what provides the kinematic viscosity. As discussed earlier, we assume that the viscosity has the form of an α viscosity (Shakura & Sunyaev 1973) so that $\nu = \alpha c_{\rm s} H$, where $c_{\rm s}$ is the disc sound speed, H is the disc scaleheight ($H = c_{\rm s}/\Omega$ with Ω the angular frequency of the disc), and $\alpha \ll 1$ is a parameter that determines the efficiency of the angular momentum transport.

We ran two sets of 100 disc models, selecting the central star mass randomly between $M_* = 0.8$ and $M_* = 1.2\,{\rm M}_\odot$. We use a ratioed grid that extends from $r = 0.1$ to $r = 1000$ au.

In one set of models, we assume the surface density of the disc model is initially non-zero inside $r = 50$ au only. When used in the population synthesis model, we assume this disc initially extends to some value of r randomly selected between 50 and 100 au, and that the fragmentation process truncates the disc to 50 au.

In the second set of models, the disc initially has non-zero surface density inside its full 100 au extent, i.e. we assume that the fragmentation process does not truncate the disc.

We assume an initial surface density profile of $\Sigma \propto r^{-1}$. Ideally, there should be a range of profiles measured: making the profile shallower may favour fragmentation by placing more mass at greater distance, which typically allows more rapid radiative cooling (Forgan & Rice 2012). In this analysis, we decided to choose a single profile to keep the scope of the work under control, but future work should investigate this.

In each simulation, the initial disc mass is randomly chosen to be between $0.125M_*$ and $0.375M_*$. The initial disc mass is therefore quite high and such discs are likely to be self-gravitating. Note that we do not add mass to the disc in any way – this is equivalent to the implicit assumption that the initial phase of cloud collapse and protostar formation is complete, and that the accretion of material on to the disc is much less than the mass-loss due to winds. This is an important assumption, as it curtails the accretion rates of the embryos, and future modelling work should address this.

Gravitationally unstable discs can either fragment to form bound objects (Boss 1998, 2002) or they can settle into a quasi-steady state in which the instability acts to transport angular momentum (Lin & Pringle 1987; Laughlin & Bodenheimer 1994).

As made clear previously, it is now reasonably well established that fragmentation is unlikely in protostellar discs within 20−30 au. If fragmentation does not take place, the GI is likely, at early times at least, to transport angular momentum outwards, allowing mass to accrete on to the central star. In such a state, the disc will achieve thermal equilibrium with dissipation due to the GI balanced by radiative cooling. Assuming $Q = 1.5$ therefore fixes the sound speed, and hence temperature, profile in the disc. It has been shown (Balbus & Papaloizou 1999; Lodato & Rice 2004) that the GI transports angular momentum in a manner analogous to viscous transport. The rate at which viscosity generates dissipation, $D(R)$, in the disc

$$D(R) = \frac{9}{4}\nu\Sigma\Omega^2 \tag{50}$$

is balanced by radiative cooling, Λ, where (Hubeny 1990)

$$\Lambda = \frac{16}{3}\sigma\left(T_c^4 - T_o^4\right)\frac{\tau}{1+\tau^2}. \tag{51}$$

In Equation (51), σ is the Stefan–Boltzmann constant, T_c is the mid-plane temperature determined from $Q = 1.5$, T_o is a temperature due to external irradiation and τ is the optical depth. We assume $\tau = \kappa\Sigma$, where κ is the opacity, and we use the analytic approximations from Bell & Lin (1994). As described in detail in Rice & Armitage (2009) (see also Clarke 2009; Zhu et al. 2009), the above can be used to determine the effective value of α. Equation (3) can therefore be integrated to determine the time evolution of Σ.

If, however, the gravitational α is less than 0.005, we assume that another transport mechanism, such as the magnetorotational instability (MRI; Balbus & Hawley 1991), will then dominate and we set $\alpha = 0.005$. In this case, we no longer require that $Q = 1.5$ but set the mid-plane temperature, T_c, such that the cooling rate given by equation (51) matches the dissipation rate given by equation (50). In addition, we also assume that irradiation from the central star sets a minimum temperature in the disc.

We also assume that radiation from the central star results in photoevaporative mass-loss, producing a disc wind ($\dot{\Sigma}_{\rm wind}$). There are a number of models for photoevaporative mass-loss, many of which assume that UV photons from the central star ionize the disc surface (e.g. Hollenbach et al. 1994; Clarke, Gendrin & Sotomayor 2001; Alexander, Clarke & Pringle 2006). Recent models, however (Owen et al. 2010), suggest that X-rays are the dominant driver and so here we implement the X-ray photoionization model described in detail in Owen et al. (2011).

Each disc model uses a different star mass, but assumes the same disc-to-star mass ratio. Despite this, the variation in X-ray luminosity (from 5×10^{28} to 10^{31} erg s^{-1}) produces a wide range of different disc lifetimes, consistent with that observed (Haisch, Lada & Lada 2001).

We therefore have a disc model that can self-consistently evolve the surface density from the early stages when the GI is likely to dominate through to the later stages when an alternative transport mechanism, such as MRI, will dominate and also includes the late-stage dispersal due to photoevaporative mass-loss.

2.3 Implementation

To conclude this section, we summarize the algorithm of the semi-analytic model.

For each planetary system, we begin by randomly selecting a disc model. We assume that either the disc truncates after fragmentation or does not. If we are dealing with a truncated disc model, we initially extend it to a maximum radius $r_{\rm max}$ beyond the model's outer radius of 50 au. We sample $r_{\rm max}$ uniformly between 50 and 100 au, and we assume that the disc surface density profile remains constant in this extension, and calculate the subsequent disc properties accordingly. If we are dealing with a non-truncated disc model (which extends to 100 au), we do not extend it in any way. Again, $r_{\rm max}$ is somewhat arbitrary – to first order, increasing $r_{\rm max}$ will increase the number of fragments initially. Whether this will increase the number of fragments that survive the tidal downsizing process is unclear. Future work should investigate how changing this affects the resulting distribution of objects.

The Jeans criterion is then used to find the minimum disc radius at which fragmentation is expected to occur. Embryos are then created, with mass equal to the local Jeans mass, at spacings of a few Hill radii (where the exact value is randomly sampled). The other initial embryo properties are calculated according to the FC equations. If we are assuming disc truncation, then we revert to the initial model, removing the material added to extend it to $r_{\rm max}$. If we do not truncate the disc, then we make no modifications at this stage.

The entire planetary system is then evolved on a timestep constrained by the physical time-scales in play. The timestep can be no larger than the minimum value of $t_{\rm gr}$, $t_{\rm sed}$ or $t_{\rm cool}$ for any embryos in the simulation. The disc model is interpolated from a look-up table to update its properties with time, and these are used to calculate the migration time-scales of all embryos. Note that each embryo is evolved independently of each other – while several embryos may be evolved in the same disc in parallel, they do not interact in any way, an important limitation (see Section 4).

Once an embryo's $t_{\rm gr}$ (which will be a function of $s_{\rm crit}$, itself a function of disc radius) has elapsed, sedimentation is allowed to proceed, and the size of the grain sphere $R_{\rm s}$ is evolved (with the sedimentation velocity not allowed to exceed 10 m s^{-1} due to fragmentation of the grains).

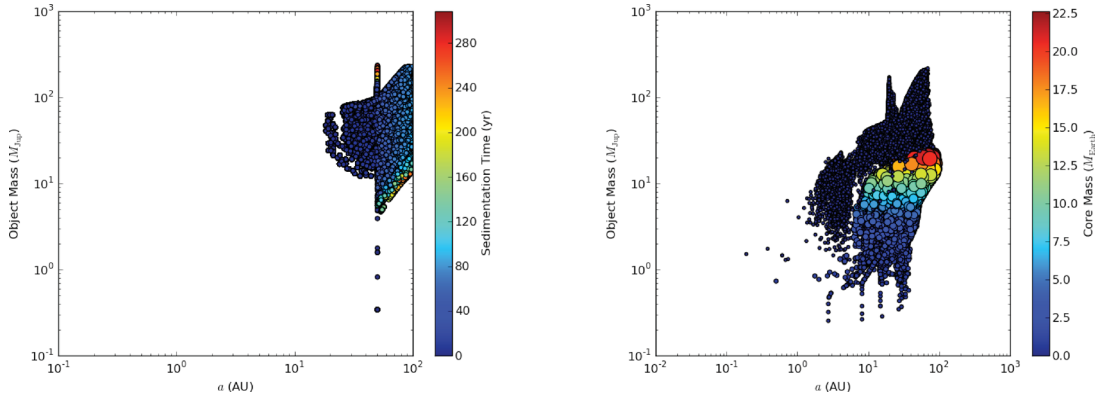

Figure 1. Embryo mass versus semimajor axis for $p_\kappa = 1$, where the disc truncates at 50 au after fragmentation. The left-hand hand panel shows the initial fragment mass–semimajor axis distribution, with the colour bar indicating the time-scale on which grains will sediment once sufficiently grown. 256 424 disc fragments were produced in this run. The right-hand panel shows the final distribution after 10^6 years. Of the fragments produced, only 116 150 survived the tidal downsizing process, and 50 543 were able to form solid cores. The colours in this plot indicate the mass of the core in Earth masses. The disc model's inner boundary is fixed at 0.1 au, and as such objects cannot cross this boundary.

At every timestep, the grain sphere is tested to check if it is self-gravitating, or self-bound. Grain spheres that are self-gravitating use the accelerated sedimentation equation, and grain spheres smaller than the Jeans length are considered to be self-bound, and immediately form solid cores.

Throughout this grain growth process, the embryo's central temperature is monitored. If the embryo exceeds temperatures of 180 K before core formation, the ice mantles are melted, and two-thirds of the solids mass is deducted from the embryo. If the temperature exceeds 1400 K, the dust is vaporized and core formation is completely halted. Embryos with temperature above 2000 K enter the second core phase and are assigned final radii according to the mass–radius relation of Burrows et al. (1997).

As the embryo migrates inwards, it will begin the process of tidal disruption. Instead of immediately stripping the embryo, the embryo's upper layers are removed more gradually over the course of one orbital period, beginning at time $t_{\rm strip}$ with the radius decaying exponentially to its Hill radius R_H according to

$$R(t) = R(t_{\rm strip}) - \left(R(t_{\rm strip}) - R_H\right) \left(1 - \exp\left(\frac{\left(t - t_{\rm strip}\right)\Omega}{2\pi}\right)\right). \quad (52)$$

The mass M of the embryo is then updated assuming the embryo remains a polytrope of index 3/2. If the new embryo radius is less than the grain sphere radius, then the total mass in solids is also reduced by an appropriate amount.

3 RESULTS

To investigate the dependence on initial input parameters, we run the population synthesis model with several different configurations.

(i) Setting $p_\kappa = 1$, and using disc models which initially extend to a radius randomly selected between 50 and 100 au, and are then immediately truncated to 50 au after fragmentation has occurred.

(ii) As (i), except that the migration time-scales are uniformly increased by a factor of 10, i.e. migration is 10 times slower.

(iii) As (i), except $p_\kappa = 2$.

(iv) As (i), except the disc models extend to 100 au, and are not truncated after fragmentation.

Every disc system is run for at least 1 Myr, to ensure the full span of disc and embryo evolution is observed.

3.1 Opacity law index $p_\kappa = 1$ (truncated disc)

The left-hand panel of Fig. 1 shows the mass–semimajor axis distribution of the embryos at the point of fragmentation. As expected, the embryos initially occupy mass ranges above a few $M_{\rm Jup}$, and fragmentation does not occur at small a. As some of the discs are quite massive and cool, the fragmentation radius can be as low as 20 au. The colour bar indicates the grain sedimentation time-scale for the embryos, which in the majority of cases is relatively short (<200 yr). If the grains can grow sufficiently quickly that sedimentation can begin before vaporization and disruption, core formation seems possible for many of the embryos.

However, the rapid temperature evolution of the embryos, coupled with tidal disruption beginning almost immediately after fragmentation, tends to prevent core formation. The right-hand panel of Fig. 1 shows the mass–semimajor axis distribution of the fragments formed in the population synthesis model after 1 Myr. Note that most embryos do not possess a solid core, and are sufficiently massive to be considered brown dwarfs. The disc inner boundary is located at 0.1 au, and as such all objects which reach this location without being tidally disrupted are not evolved any further.

There is a lack of objects at semimajor axes below ∼5 au – somewhat consistent with the 'brown dwarf desert' (Halbwachs et al. 2000; Marcy & Butler 2000) – which can be seen in the right-hand panel of Fig. 2. Generally, objects above the brown dwarf mass limit exist at semimajor axes >20 au, showing that in situ formation of brown dwarfs via fragmentation remains viable in the tidal downsizing paradigm, in agreement with recent numerical simulations (Stamatellos & Whitworth 2009; Kaplan, Stamatellos & Whitworth 2012).

If we consider both histograms in Fig. 2, we can see that attrition of the embryo thanks to tidal disruption, and the loss of embryos through migration strongly shapes the final statistics of the objects. Around 40 per cent of all embryos formed are lost – as the mass of the embryo decreases during the disruption process, the migration

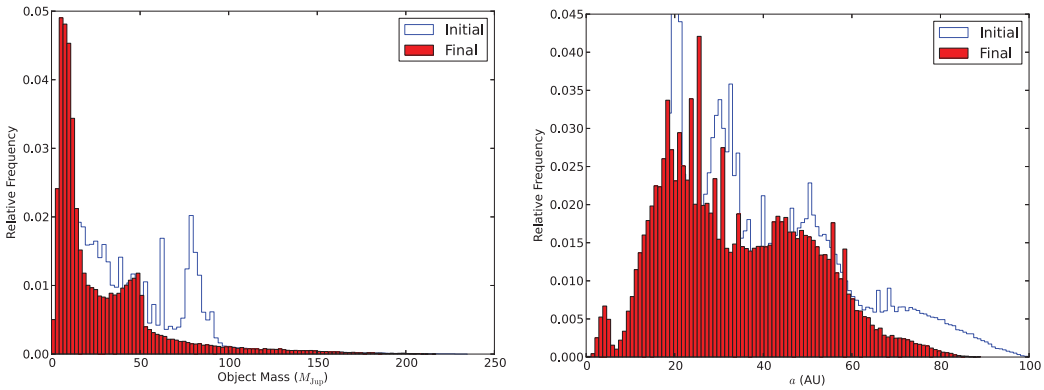

Figure 2. Comparing the initial (blue lines) and final (red bars) distributions of embryo mass (left) and embryo semimajor axis (right).

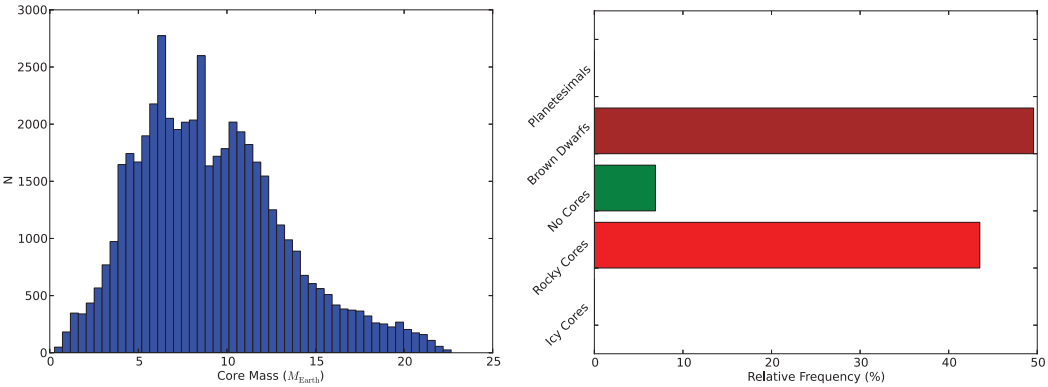

Figure 3. Left: the distribution of core masses after 10^6 years of evolution. Right: the relative frequency of each object type formed in the population synthesis model.

regime switches from type II to type I, significantly reducing the migration time-scale and forcing objects towards the central star. The mass distribution of objects (left-hand panel of Fig. 2) shows a significant number of objects formed above 50 $M_{\rm Jup}$, with masses in the hydrogen-burning M dwarf regime, but the final mass distribution tends to fall off above this value as disruption acts on these embryos before nuclear reactions begin.

While there are some embryos with final semimajor axes below 10 au (right-hand panel of Fig. 2), the relative frequency of objects is quite low. Indeed, the final semimajor axis distribution retains a strong signature of the minimum fragmentation radius of about 20 au. Despite this fragmentation boundary being much closer to the central star than the values of 40–70 au typically found in numerical simulations, the population of close-in objects remains quite small compared to the large semimajor axis population. This appears to be due to disc truncation – as most of the objects will form in regions that have experienced truncation, they will not begin migration until the disc has spread on viscous time-scales. This increases the migration time-scale, and allows them to evolve with limited tidal disruption and reach the 'second collapse' due to H_2 dissociation before the disc can act to move the objects inwards, and increase the rate of tidal disruption.

The left-hand panel of Fig. 3 shows the distribution of solid core masses formed in this run. The distribution is peaked at around 6 $M_\oplus$, with a tail extending as far as 22 $M_\oplus$. The extrema of the distribution compares well to (for example) the range of estimates for Jupiter's core mass (0–18 $M_\oplus$; Guillot 1999; Nettelmann 2011), but we must also remember that objects formed in the model with these core masses are likely to have total masses of 10 $M_{\rm Jup}$ or above.

The right-hand panel of Fig. 3 illustrates that brown dwarfs are the most populous of all the surviving objects in this run (around 50 per cent of the total), closely followed by objects with a solid core (at around 42 per cent). No icy cores are formed, as the embryos quickly exceed the melting temperature before core formation. If and when the grain growth process is successful, the sedimentation time-scale is sufficiently short that cores are formed before full disruption occurs. We should therefore conclude that (for these parameters) these disruption events do not add significant processed materials or sub Earth mass solid bodies to the surrounding environment.

3.2 Opacity law index $p_\kappa = 1$ (truncated disc, inefficient migration)

In the same vein as Ida & Lin (2008), we now vary the speed of migration by multiplying the migration time-scales in equations (46) and (47) by a factor of 10. Fig. 4 shows the initial and final mass versus semimajor axis distributions in this run.

With migration 10 times less efficient than the previous run, semimajor axes lower than the fragmentation boundary are less

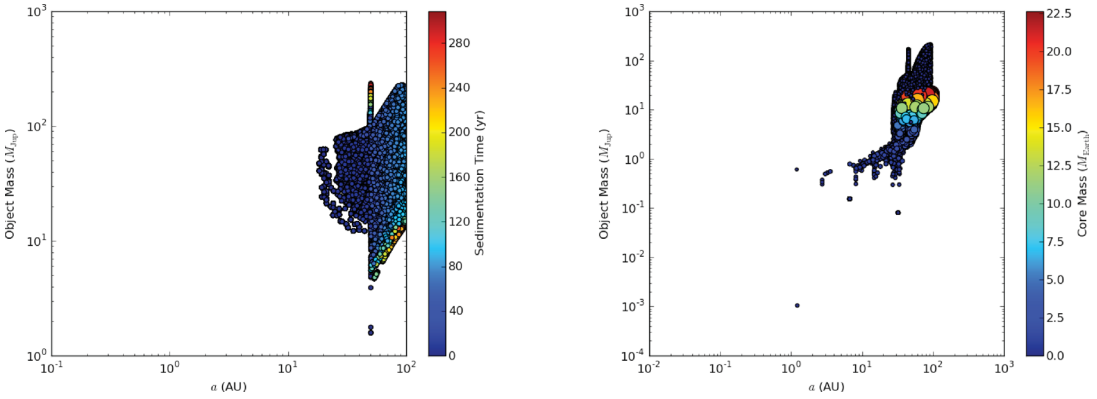

Figure 4. Embryo mass versus semimajor axis for $p_\kappa = 1$, with a disc that truncates at 50 au after fragmentation and migration time-scales increased by a factor of 10. The left-hand panel shows the initial fragment mass–semimajor axis distribution, with the colour bar indicating the time-scale on which grains will sediment once sufficiently grown. 202 385 disc fragments were produced in this run. The right-hand panel shows the final distribution after 10^6 years. Of the fragments produced, only 92 295 survived the tidal downsizing process, and 40 571 were able to form solid cores. The colours in this plot indicate the mass of the core in Earth masses.

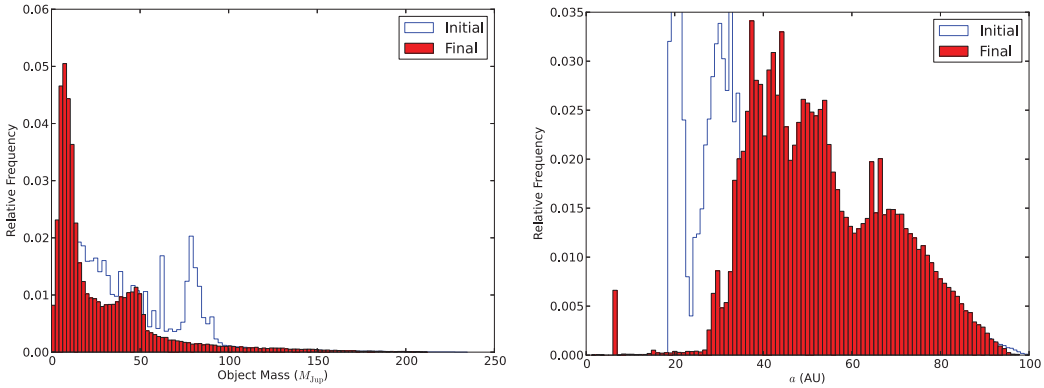

Figure 5. Comparing the initial (blue lines) and final (red bars) distributions of embryo mass (left) and embryo semimajor axis (right).

populated than before. Some objects still migrate to the disc inner boundary, but in much fewer numbers than before. The sedimentation time-scale for the fragments remains the same, so the cores produced are very similar to the previous case. With the ratio between sedimentation and migration time-scale being reduced by a factor of 10, the formation of solid cores before disruption is somewhat easier. Indeed, this run shows the only example of a terrestrial planet being formed in the simulation, with mass less than 1 $M_\oplus$ at a semimajor axis of 1 au.

The embryo mass distribution (Fig. 5, left-hand panel) remains relatively unchanged, but the semimajor axis distribution (right-hand panel) shows an even larger desert, with few objects ending up inside 20 au.

The core mass distribution (left-hand panel of Fig. 6) is again very similar as the sedimentation behaviour is unchanged. Brown dwarfs still dominate the population (right-hand panel of Fig. 6), followed closely by cored objects.

3.3 Opacity law index $p_\kappa = 2$ (truncated disc)

In this run, we now allow migration to be efficient, and truncate the disc at fragmentation, but change the opacity law so that it scales with the square of the temperature. This significantly increases the cooling time of the embryo, which will have important consequences for the population produced. Fig. 7 shows the initial and final mass versus semimajor axis distributions for this run.

The inefficient cooling of the embryo results in a greatly increased destruction rate – over 95 per cent of the fragments produced in this run are destroyed. Only the most massive objects survive, and there are only a handful that survive in the inner disc. This is reflected in the mass and semimajor axis distributions (Fig. 8).

Perhaps most worrying are the extremely large solid core masses produced in this run (left-hand panel of Fig. 9). The mode of this distribution is around 200 $M_\oplus \sim 0.5\,M_{\rm Jup}$. Note that these very large cores only exist in massive gaseous embryos – there are no terrestrial-type objects (i.e. solid cores without gaseous envelopes). These anomalously large cores are suggestive of missing physics from the model (see Section 4).

The inefficiency of embryo cooling only allows massive objects to remain bound without becoming disrupted, and as a result cores form very rarely in this run (only around 10 per cent of all surviving objects). The other 90 per cent form brown dwarfs – indeed, some are massive enough to form hydrogen-burning low-mass stars with masses $\sim$0.1 $M_\odot$.

3.4 Opacity law index $p_\kappa = 1$ (no disc truncation)

We have seen in the previous runs that the migration of the embryos strongly determines their mass and semimajor axis evolution. Until

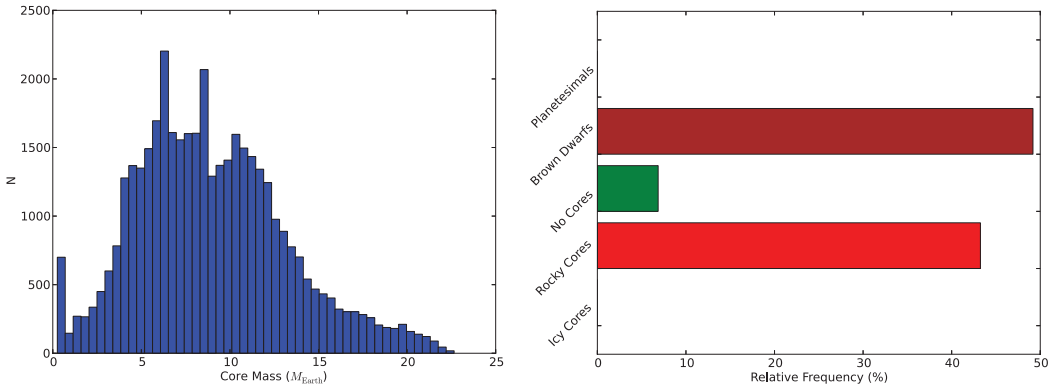

Figure 6. Left: the distribution of core masses after 10^6 years of evolution. Right: the relative frequency of each object type formed in the population synthesis model.

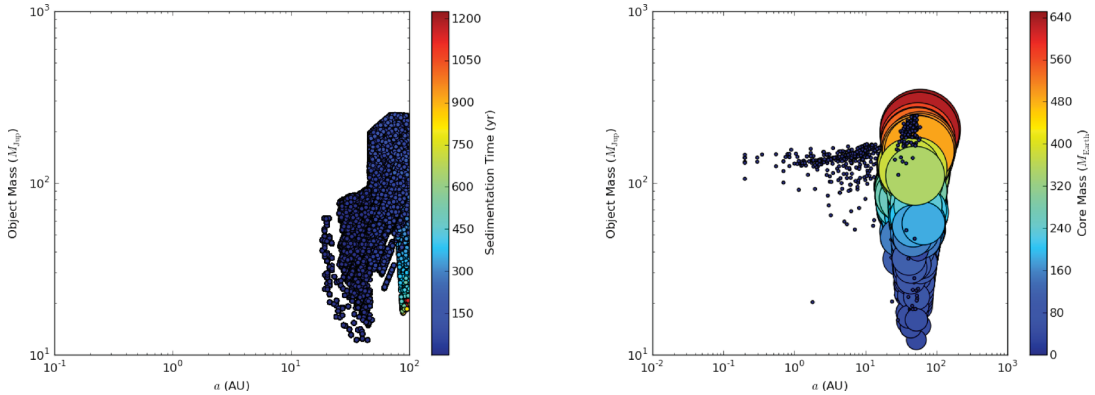

Figure 7. Embryo mass versus semimajor axis for $p_\kappa = 2$, with a disc that truncates at 50 au after fragmentation. The left-hand panel shows the initial fragment mass–semimajor axis distribution, with the colour bar indicating the time-scale on which grains will sediment once sufficiently grown. 530 488 disc fragments were produced in this run. The right-hand panel shows the final distribution after 10^6 years. Of the fragments produced, only 22 637 survived the tidal downsizing process, and 2292 were able to form solid cores. The colours in this plot indicate the mass of the core in Earth masses. The left-hand panel shows the initial fragment mass–semimajor axis distribution, with the colour bar indicating the time-scale on which grains will sediment once sufficiently grown.

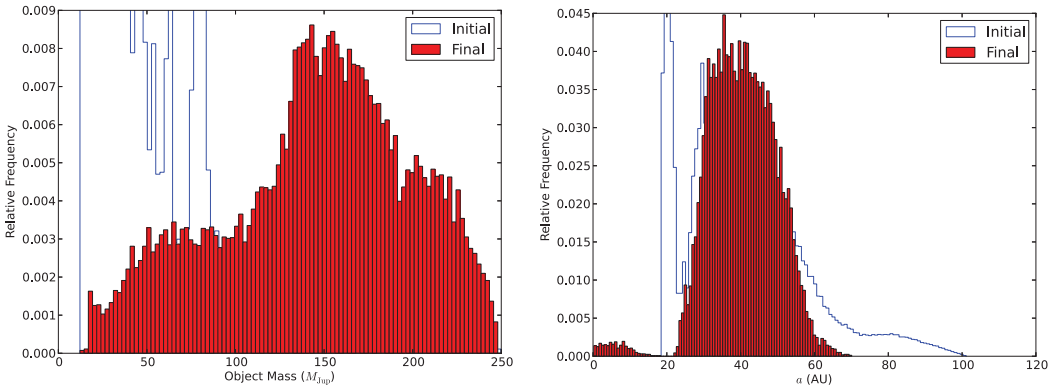

Figure 8. Comparing the initial (blue lines) and final (red bars) distributions of embryo mass (left) and embryo semimajor axis (right).

now, we have assumed that the fragmentation process truncates the disc, which allows embryos to evolve their physical radius and dust population before the disc can undergo viscous spreading, extending its outer radius until it encroaches upon their orbital domains, and begin the migration process.

In this run, we do not truncate the disc at fragmentation. The disc can therefore begin migrating the embryos immediately, decreasing the Hill radius of the embryos precipitately and significantly increasing the rate of disruption. As the $p_\kappa = 2$ run already shows a high destruction rate, we reset p_κ to 1 to assess the significance of disc truncation.

Fig. 10 shows the initial and final mass versus semimajor axis distributions, which indicate that removing disc truncation has a significant effect. Again, there are no terrestrial-type objects, and

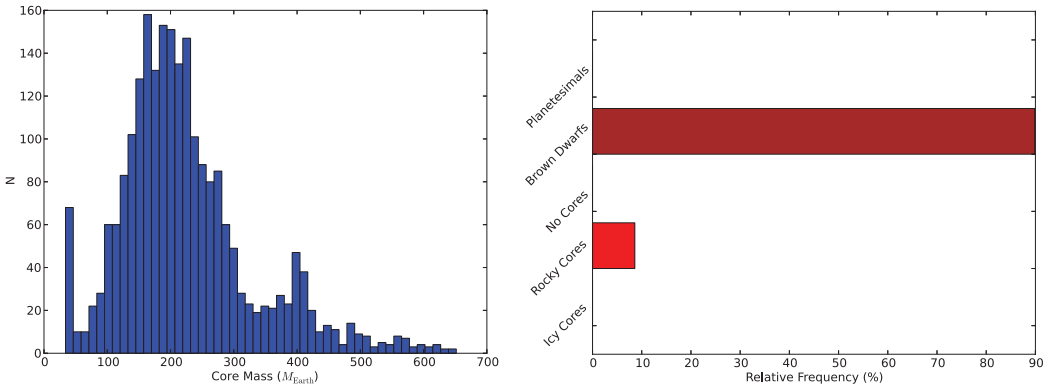

Figure 9. Left: the distribution of core masses after 10^6 years of evolution. Right: the relative frequency of each object type formed in the population synthesis model.

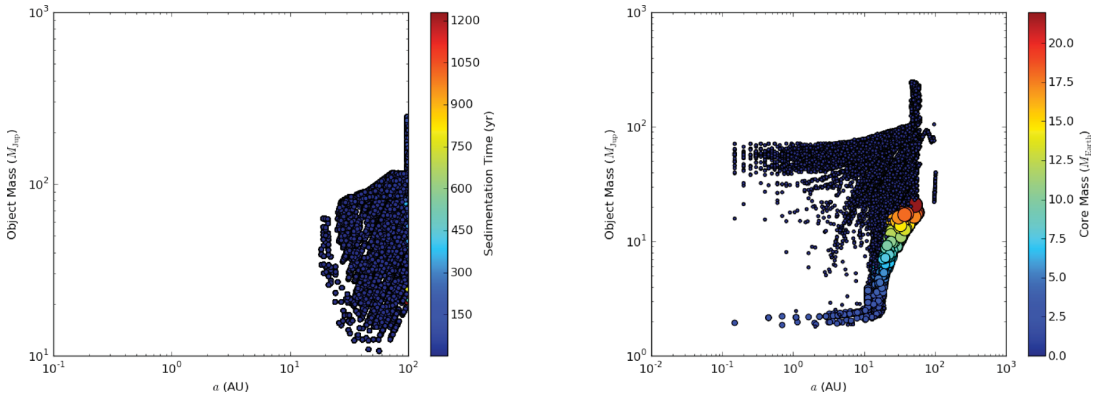

Figure 10. Embryo mass versus semimajor axis for $p_\kappa = 1$, with a disc that does not truncate after fragmentation. The left-hand panel shows the initial fragment mass–semimajor axis distribution, with the colour bar indicating the time-scale on which grains will sediment once sufficiently grown. 205 184 disc fragments were produced in this run. The right-hand panel shows the final distribution after 10^6 years. Of the fragments produced, only 74 430 survived the tidal downsizing process, and 7378 were able to form solid cores. The colours in this plot indicate the mass of the core in Earth masses. The left-hand panel shows the initial fragment mass–semimajor axis distribution, with the colour bar indicating the time-scale on which grains will sediment once sufficiently grown.

all objects which possess a core possess a massive envelope. With migration occurring immediately after fragmentation, many more objects reach the inner disc boundary, producing a small population of Hot Jupiters and close BD companions. Core formation is suppressed compared to the other $p_\kappa = 1$ runs: cores form in 10 per cent of surviving embryos compared to around 40 per cent in the other p_κ cases.

The mass distribution of the objects (left-hand panel of Fig. 11) remains relatively unchanged from initial to final, forming large numbers of objects up to $100\,M_{\rm Jup}$. The two modes of the distributions are generated by the spacing of the fragments as they form in the disc (with some broadening of the peaks due to the uniform sampling of the spacing in Hill radii described in earlier sections).

This population is very much a stellar population. The brown dwarf desert is less significant (right-hand panel of Fig. 11), and few objects survive with semimajor axis larger than 60 au.

The core mass distribution (left-hand panel of Fig. 12) also reflects the initial mass distribution. Less than 10 per cent of all surviving objects have cores (right-hand panel of Fig. 12), and nearly 90 per cent of all the objects are brown dwarfs (or low-mass stars).

4 DISCUSSION

4.1 Limitations of the model

We readily admit that this model, while detailed in construction, still lacks some important physics, which we hope to include in future work.

4.1.1 Accretion of mass and angular momentum by the embryo

Perhaps the most glaring omission from this population synthesis model is accretion of material on to the embryos after fragmentation. As the semi-analytic disc model is evolved without the presence of fragments, modelling subsequent mass-loss from the disc on to embryos is not possible. The embryo should be able to accrete provided it does not open a significant gap, which it will do if (a) its Hill radius exceeds the local disc scale-height and (b) the clump is sufficiently massive to overcome the local Reynolds turbulence (Lin & Papaloizou 1979). For almost all fragments formed, this criterion is easily satisfied initially. However, as the embryo migrates inwards, the Hill radius decreases, and the embryo's mass also decreases due to tidal disruption. The gap

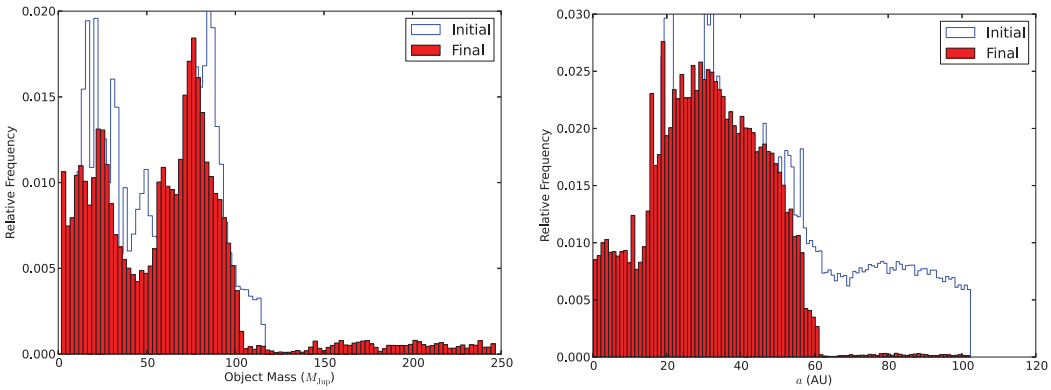

Figure 11. Comparing the initial (blue lines) and final (red bars) distributions of embryo mass (left) and embryo semimajor axis (right).

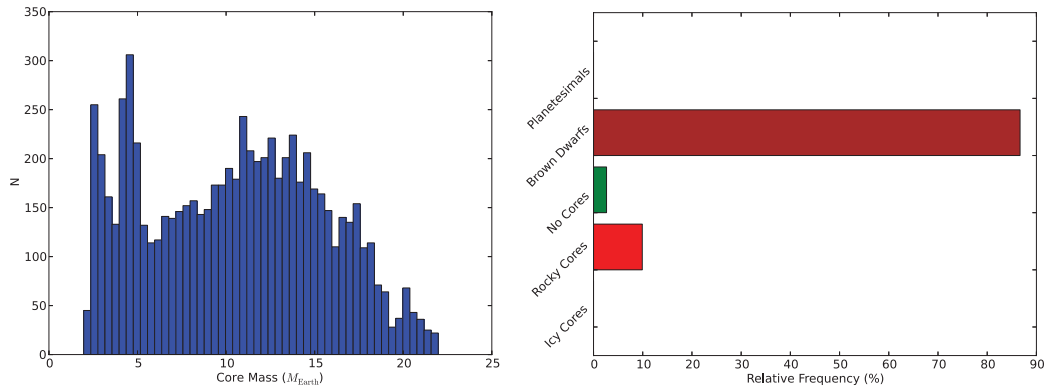

Figure 12. Left: the distribution of core masses after 10^6 years of evolution. Right: the relative frequency of each object type formed in the population synthesis model.

opening criterion will no longer be satisfied, and accretion can begin once more.

To what level this latter accretion phase will affect the subsequent evolution of fragments is unclear. Numerical simulations by Zhu et al. (2012) show gap opening at semimajor axes as low as 10 au, which would be a consequence of accretion increasing the Hill radius past the value of the local scale-height.

We have also ignored the embryo's ability to accrete solids from its surroundings (Helled et al. 2006; Helled & Bodenheimer 2010). The embryo may be able to substantially enrich itself during the early stages of its contraction, accreting a large fraction of the available planetesimals in its feeding zone, boosting the dust-to-gas ratio. This could be incorporated into our model quite simply using simple two-body capture approximations.

The accretion history of the embryo will determine its angular momentum. Cha & Nayakshin (2011) find in their numerical simulations that the fragments produced rotate prograde to the disc's rotation, with a rotational angular frequency approximately 10 per cent of their maximum break-up frequency. This can be used to estimate the rotational angular frequency of terrestrial planets formed from these embryos whose maximum exceeds the break-up frequency (Nayakshin 2011a). This would suggest that embryos rotate sufficiently rapidly to form circumembryonic discs (Boley et al. 2010; Shabram & Boley 2013) and binary cores, an outcome not producible in this current model.

Equally, the rotation rate of giant planets is expected, as a rule, to be initially prograde, and close to the break-up frequency, although stellar tides can damp this rotation rate. Also, events such as planet–planet scattering or the Kozai mechanism can produce retrograde orbits (e.g. Nagasawa & Ida 2011). Future work should model this angular momentum evolution in detail.

4.1.2 Dust coagulation

The extremely massive cores produced by the $p_\kappa = 2$ run suggest that there is missing physics in the coagulation of the dust grains. While turbulence is part of the coagulation process in these models, convection is not. As we have mentioned previously, allowing the envelope to be convective can significantly increase the sedimentation time-scale (Helled et al. 2008), although it does not completely preclude core formation, especially for low-mass embryos (Helled & Schubert 2008). Also, we should strictly alter the opacity in the embryo as the grains sediment, as the local metallicity of the gas can change significantly. Global metallicity effects are also important: decreasing the initial dust-to-gas ratio in the disc can greatly decrease the contraction time-scale of the embryo (Helled & Bodenheimer 2011).

4.1.3 Embryo migration

We have deliberately implemented a basic model of planetary migration in this work, as this allows us to investigate the complete system of equations presented by Nayakshin (2010b, 2011b,c) and

assess their expected output on a statistical level. As such, the modelling of migration misses out important characteristics of the migration process: stochasticity due to disc turbulence (Baruteau et al. 2011), resonant migration of multiple bodies (e.g. Libert & Tsiganis 2011) and halting of migration at planet traps induced by disc structure (e.g. Kretke & Lin 2012). Inwardly migrating giant planets can even halt or reverse the motion of low-mass planets at larger semimajor axis (Podlewska-Gaca, Papaloizou & Szuszkiewicz 2012).

Also, the eccentricity and inclination evolution of the bodies is not tracked: recent numerical simulations suggest that eccentricity excitation via planet–disc interaction will be low for planet masses of a few Jupiter masses (Dunhill, Alexander & Armitage 2012), which appears to be borne out by observations (Dawson, Murray-Clay & Johnson 2012), but future models should investigate this by allowing eccentricities to be excited and damped.

Most migration models are developed for low-mass, non-self-gravitating discs: simulations of fragment migration in self-gravitating discs have shown that the usual embryo migration equations do not appear to apply, and that fragment migration is typically much faster (Baruteau et al. 2011; Michael et al. 2011; Zhu et al. 2012). Also, as our embryos are evolved independently of each other, we cannot model for example the chaotic orbital interchanges witnessed in self-gravitating disc simulations with multiple embryos (Boss 2013). It is unclear how these interactions can be modelled semi-analytically, but it is clear that any model output should be considered with the absence of this physical process at the forefront of one's mind.

Can these simulations produce semi-analytic prescriptions for migration? Baruteau et al. (2011) show that gravitoturbulence reduces the type I migration time-scale by a factor of a few as a result of the disc's non-axisymmetry pushing the location of Lindblad resonances towards the planet. Zhu et al. (2012) also show that the type I time-scale is altered by a factor which they fitted in terms of embryo mass and local surface density, accounting for the embryo's inertia. Future modelling should consider implementing some of these initial empirical results.

4.2 Terrestrial planet formation via tidal downsizing

Despite the above limitations, we can make some reasonably robust statements regarding the likelihood of terrestrial planet formation. All the runs carried out in this paper show that planets of mass $\sim \mathrm{M}_{\oplus}$ are extremely rare – out of over a million disc fragments, only one stands out as a clear example of a terrestrial planet.

Most of the missing physics described above is likely to inhibit the formation of low-mass cores rather than encourage it, so future population synthesis modelling is likely to produce even fewer terrestrial planets than we see here. In short, it appears to be clear that while GI followed by tidal downsizing can produce terrestrial planets on some occasions, it is not an efficient means of constructing such objects. This would indicate that terrestrial planets are much more likely to be formed by CA than disc fragmentation.

4.3 Production of asteroid belts

For the production of asteroid belts via tidal downsizing, the grain growth process must be well advanced, without the sedimentation process forming a solid core or the embryo temperature increasing above the vaporization temperature. If the disruption process is sufficiently rapid, then the embryo and core will unbind, and the grains in the embryo will be distributed in a ring at the semimajor axis where disruption began (Nayakshin & Cha 2012).

In these models, we did not see any embryos which completely satisfy the above conditions for belt formation. Only one run (the non-truncated $p_\kappa = 1$ run) showed some embryos with grains surviving the disruption process without either being vaporized or forming a core. The embryos showed evidence of ice melting, but their grains had not grown to the point where sedimentation would begin. As such, these would not form asteroid belts in the conventional sense, but could perhaps form dust belts with some grains already grown (cf. Boley et al. 2010).

This would skew the disc grain size distribution towards larger values, potentially providing a 'shortcut' to grain growth in the CA model. This enhanced grain growth is similar to the grain growth observed in non-fragmenting self-gravitating disc spiral structures, which has also been proposed as a means of accelerating the CA process (Rice et al. 2004; Gibbons, Rice & Mamatsashvili 2012). The key difference between embryo-enhanced grain populations and spiral-wave-enhanced populations is the location of the grains' deposition: spiral-wave-enhanced grains will occupy semimajor axes above several tens of au (Clarke & Lodato 2009), whereas embryo-enhanced grains can be delivered to lower semimajor axis before the embryo is destroyed.

If sedimentation has just begun when the embryo is totally disrupted, then a large fraction of the grains supplied to the disc may be of order millimetre sizes, allowing rapid CA (Lambrechts & Johansen 2012).

4.4 Embryo disruption and protostellar outburst models

In this work, typically around 40 per cent of all embryos were completely destroyed by tidal disruption. This large destruction rate, borne out by numerical simulations (e.g. Boley & Durisen 2010; Nayakshin 2010a,b, 2011b; Zhu et al. 2012), could result in protostellar outburst behaviour such as the FU Orionis phenomenon (Vorobyov & Basu 2005, 2006; Dunham & Vorobyov 2012). If this is the case, then the behaviour of the gas as it becomes unbound from the embryo will determine the nature of the burst. Indeed, subsequent disc fragmentation can be suppressed by the star's outburst (Stamatellos, Whitworth & Hubber 2012). We have not coupled disc evolution and embryo evolution, and so we cannot model such behaviour. As a result, the population synthesis model does not characterize the outbursts, but merely suggests that episodic stellar accretion is a common outcome of the disc fragmentation process.

More subtly, Nayakshin & Lodato (2012) show how a tidally disrupting embryo can create deep gaps in the inner disc that are refilled by its own matter, which can then be accreted on to the central star, producing outbursts and quiescent periods as the gap refills, without the embryo's destruction (see also Lodato & Clarke 2004). While this population synthesis model does not self-consistently evolve the embryo evolution and the disc evolution, this phenomenon could be modelled semi-analytically in the future.

4.5 Brown dwarfs and the desert

The population synthesis model predominantly produces brown dwarfs – this is true for all four runs carried out in this work. Depending on the opacity law, as much as 90 per cent of the objects that survive the tidal downsizing process satisfy the canonical $M > 13\,M_{\mathrm{Jup}}$ criterion for being brown dwarfs. Does the brown dwarf desert (Halbwachs et al. 2000; Marcy & Butler 2000) survive the migration process? In Fig. 13, we plot the semimajor axis distribution of the brown dwarfs formed in all four runs.

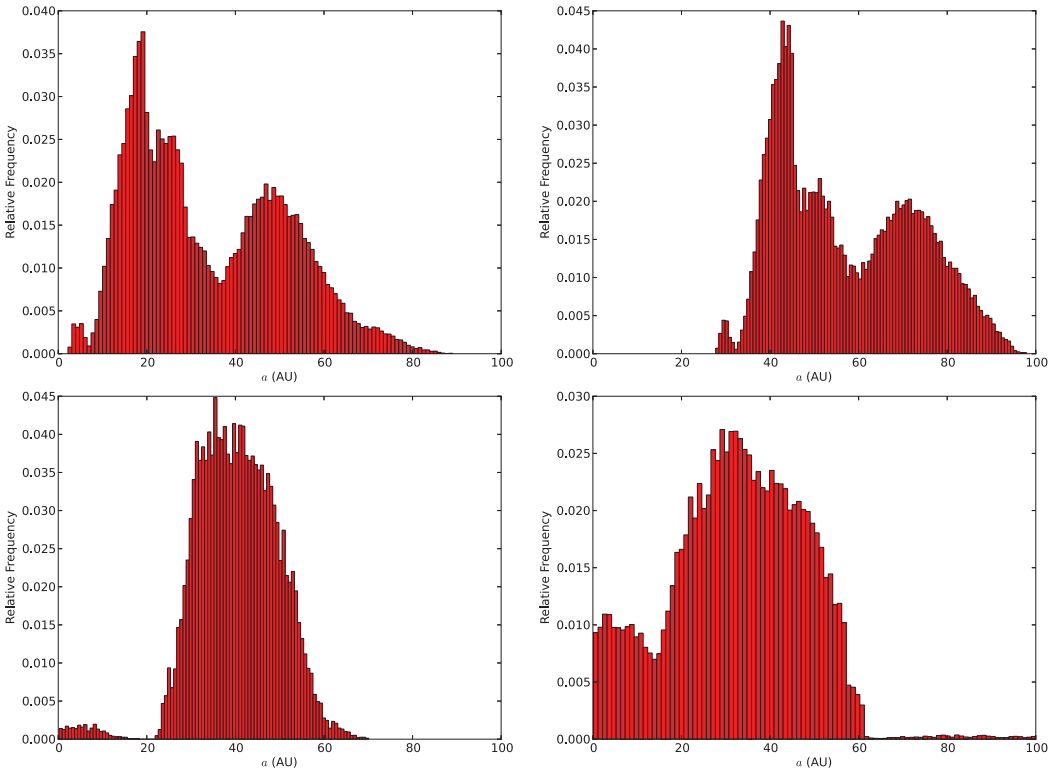

Figure 13. The final semimajor axis distribution of all brown dwarfs for the four runs carried out in this work.

If we define the desert as a lack of objects below around 5 au, then the runs with $p_\kappa = 1$ and disc truncation show this lack quite strikingly. If migration is suppressed (top right of Fig. 13), then this desert extends as far as the fragmentation boundary of the disc model. Changing the opacity law or not truncating the disc makes the desert less striking – brown dwarfs are then able to survive to the inner edge of the disc model at 0.1 au. The $p_\kappa = 2$ run still preserves a desert in between $0.2 < r < 20$ au, but the run without disc truncation shows a desert with greatly reduced significance.

This would suggest that for a strong brown dwarf desert to be formed, the disc should truncate during the fragmentation process (or migration should be inefficient), and the embryo's opacity should not increase too quickly with temperature. We do not fully model the so-called 'opacity gap' normally seen at temperatures between ∼500 and 5000 K (e.g. Bell & Lin 1994), which would significantly affect the collapse of the embryo envelope. A new set of grain growth and sedimentation equations where p_κ is allowed to vary with temperature would also significantly affect the potential for core formation.

Also, we do not model ejection of brown dwarfs via scattering or three-body interactions (Bate et al. 2003; Goodwin & Whitworth 2007), which may be more efficient at removing coreless objects than objects with cores (Liu et al. 2012). Regardless, our results would suggest that the destruction of inwardly migrating brown-dwarf-mass objects is already quite efficient at removing close separation brown dwarf companions (Armitage & Bonnell 2002), and that the restriction of disc fragmentation to semimajor axes well above 5 au would ensure those brown dwarfs which survive disruption would be unlikely to form close separation binaries with their parent star.

5 CONCLUSIONS

We have presented the first attempt at a population synthesis model for objects produced by self-gravitating disc fragmentation and subsequent tidal downsizing. The model imposes a protoplanetary disc, which can then fragment under FI. The fragments can then migrate, grow grains, sediment those grains to the centre of the fragment and form solid cores, or be tidally disrupted (not necessarily in that order). Each protoplanetary disc (if it fragments) produces several objects – running the model many times with different disc properties produces a large number of objects, allowing the construction of statistics on tidal downsizing as a planet formation mode.

We ran the population synthesis model for four different scenarios, varying the speed of migration, how the opacity within the embryo changes with temperature and whether the fragmentation process truncates the disc or not. Each run simulates a sufficient number of discs to produce $\sim 10^5$ fragments.

In general, we find that around half of all fragments are completely destroyed during the tidal downsizing process. The majority of surviving fragments remain at semimajor axes >20 au after 1 Myr of evolution. Their masses are typically greater than $5\,M_{\rm Jup}$, with a large fraction exceeding the brown dwarf mass limit of $13\,M_{\rm Jup}$. Solid cores form with a distribution of masses peaked typically at $6\,{\rm M}_\oplus$. Only a very small fraction of these solid cores lose their outer envelopes to form terrestrial planets (<0.001 per cent). We see no production of planetesimal belts via evolved grain populations becoming unbound during the destruction of the embryo (although we saw some weak evidence of processed solids being returned to the disc via disruption).

The model process does require further development, and the physics to be added will both suppress and enhance grain growth/core formation. More appropriate migration models may speed up the tidal disruption process (Baruteau et al. 2011), but equally more faithful modelling of enrichment at birth (Boley & Durisen 2010) planetesimal capture (Helled et al. 2006) and opacity evolution during embryo contraction (Helled & Bodenheimer 2011) can produce cores much more rapidly (Helled et al. 2008; Helled & Bodenheimer 2011). In short, it remains possible that the GI mode of planet formation can form a modest number of terrestrial planets, but it appears to form a much larger quantity of giant planets and brown dwarfs that preferentially exist at semimajor axes above around 30 au.

ACKNOWLEDGEMENTS

DF and KR gratefully acknowledge support from STFC grant ST/J001422/1. The authors wish to thank Sergei Nayakshin for useful discussions regarding the construction of this model, and the referee for their comments which greatly strengthened and balanced this paper.

REFERENCES

Alexander R. D., Clarke C. J., Pringle J. E., 2006, MNRAS, 369, 229
Alibert Y., Mordasini C., Benz W., Winisdoerffer C., 2005, A&A, 434, 343
Armitage P. J., Bonnell I. A., 2002, MNRAS, 330, L11
Armitage P. J., Livio M., Pringle J. E., 2001, MNRAS, 324, 705
Artymowicz P., 1993, ApJ, 419, 166
Balbus S. A., Hawley J. F., 1991, ApJ, 376, 214
Balbus S. A., Papaloizou J., 1999, ApJ, 521, 650
Baruteau C., Masset F., 2013, in Souchay J., Mathis S., Tokieda T., eds, Lecture Notes in Physics, Vol. 861, Tides in Astronomy and Astrophysics. Springer, Berlin
Baruteau C., Meru F., Paardekooper S.-J., 2011, MNRAS, 416, 1971
Bate M. R., Bonnell I. A., Bromm V., 2003, MNRAS, 339, 577
Bell K. R., Lin D. N. C., 1994, ApJ, 427, 987
Bitsch B., Kley W., 2010, A&A, 523, A30
Bitsch B., Boley A., Kley W., 2013, A&A, 550, A52
Blum J., Wurm G., 2008, ARA&A, 46, 21
Boley A. C., 2009, ApJ, 695, L53
Boley A. C., Durisen R. H., 2010, ApJ, 724, 618
Boley A. C., Hayfield T., Mayer L., Durisen R. H., 2010, Icarus, 207, 509
Boley A. C., Mejia A. C., Durisen R., Cai K., Pickett M. K., D'Alessio P., 2006, ApJ, 651, 517
Boley A. C., Helled R., Payne M. J., 2011, ApJ, 735, 30
Boss A. P., 1997, Sci, 276, 1836
Boss A. P., 1998, ApJ, 503, 923
Boss A. P., 2002, ApJ, 576, 462
Boss A. P., 2013, ApJ, 764, 194
Burrows A. et al., 1997, ApJ, 491, 856
Burrows A., Heng K., Nampaisarn T., 2011, ApJ, 736, 47
Cameron A. G. W., 1978, Moon Planets, 18, 5
Cha S.-H., Nayakshin S., 2011, MNRAS, 415, 3319
Clarke C. J., 2009, MNRAS, 396, 1066
Clarke C. J., Gendrin A., Sotomayor M., 2001, MNRAS, 328, 485
Clarke C. J., Harper-Clark E., Lodato G., 2007, MNRAS, 381, 1543
Clarke C. J., Lodato G., 2009, MNRAS, 398, L6
Cossins P., Lodato G., Clarke C. J., 2009, MNRAS, 393, 1157
Dawson R. I., Murray-Clay R. A., Johnson J. A., 2012, preprint (arXiv:1211.0554)
Dullemond C. P., Dominik C., 2005, A&A, 434, 971
Dunham M. M., Vorobyov E. I., 2012, ApJ, 747, 52
Dunhill A., Alexander R., Armitage P., 2012, MNRAS, 428, 3072
Durisen R., Boss A. P., Mayer L., Nelson A. F., Quinn T., Rice W. K. M., 2007, in Reipurth B., Jewitt D., Keil K., eds, Protostars and Planets V, Gravitational Instabilities in Gaseous Protoplanetary Disks and Implications for Giant Planet Formation. University of Arizona Press, Tucson, p. 607
Forgan D., Rice K., 2011, MNRAS, 417, 1928
Forgan D., Rice K., 2012, MNRAS, 420, 299
Forgan D., Rice K., 2013, MNRAS, 430, 2082
Forgan D. H., Rice K., Stamatellos D., Whitworth A. P., 2009, MNRAS, 394, 882
Forgan D., Rice K., Cossins P., Lodato G., 2011, MNRAS, 410, 994
Fouchet L., Alibert Y., Mordasini C., Benz W., 2012, A&A, 540, A107
Fromang S., Papaloizou J., 2006, A&A, 452, 751
Gammie C., 2001, ApJ, 553, 174
Gibbons P. G., Rice W. K. M., Mamatsashvili G. R., 2012, MNRAS, 426, 1444
Goodwin S. P., Whitworth A., 2007, A&A, 466, 943
Guillot T., 1999, Planet. Space Sci., 47, 1183
Güttler C., Blum J., Zsom A., Ormel C. W., Dullemond C. P., 2010, A&A, 513, A56
Haisch J., Lada E. A., Lada C. J., 2001, ApJ, 553, L153
Halbwachs J. L., Arenou F., Mayor M., Udry S., Queloz D., 2000, A&A, 355, 581
Helled R., Bodenheimer P., 2010, Icarus, 207, 503
Helled R., Bodenheimer P., 2011, Icarus, 211, 939
Helled R., Schubert G., 2008, Icarus, 198, 156
Helled R., Podolak M., Kovetz A., 2006, Icarus, 185, 64
Helled R., Podolak M., Kovetz A., 2008, Icarus, 195, 863
Hollenbach D., Johnstone D., Lizano S., Shu F., 1994, ApJ, 428, 654
Hopkins P. F., Christiansen J. L., 2013, preprint (arXiv:1301.2600)
Hubeny I., 1990, ApJ, 351, 632
Hubickyj O., Bodenheimer P., Lissauer J., 2005, Icarus, 179, 415
Ida S., Lin D. N. C., 2004, ApJ, 604, 388
Ida S., Lin D. N. C., 2008, ApJ, 673, 487
Kaplan M., Stamatellos D., Whitworth A. P., 2012, Astrophys. Space Sci., 341, 395
Kley W., Nelson R., 2012, ARA&A, 50, 211
Kratter K. M., Murray-Clay R. A., 2011, ApJ, 740, 1
Kratter K. M., Murray-Clay R. A., Youdin A. N., 2010, ApJ, 710, 1375
Kretke K. A., Lin D. N. C., 2012, ApJ, 755, 74
Lambrechts M., Johansen A., 2012, A&A, 544, A32
Laughlin G., Bodenheimer P., 1994, ApJ, 436, 335
Libert A.-S., Tsiganis K., 2011, Celest. Mech. Dyn. Astron., 111, 201
Lin D. N. C., Papaloizou J., 1979, MNRAS, 186, 799
Lin D. N. C., Pringle J. E., 1987, MNRAS, 225, 607
Lissauer J. J., 1987, Icarus, 69, 249
Lissauer J. J. et al., 2011, Nat, 470, 53
Liu S.-F., Guillochon J., Lin D. N. C., Ramirez-Ruiz E., 2012, ApJ, 762, 37
Lodato G., Clarke C. J., 2004, MNRAS, 353, 841
Lodato G., Clarke C. J., 2011, MNRAS, 413, 2735
Lodato G., Rice W. K. M., 2004, MNRAS, 351, 630
Low C., Lynden-Bell D., 1976, MNRAS, 176, 367
Lynden-Bell D., Pringle J. E., 1974, MNRAS, 168, 603
Marcy G., Butler R., 2000, PASP, 112, 137
Masunaga H., Inutsuka S., 1999, ApJ, 510, 822
Masunaga H., Miyama S. M., Inutsuka S., 1998, ApJ, 495, 346
Matzner C. D., Levin Y., 2005, ApJ, 628, 817
Meru F., Bate M. R., 2011, MNRAS, 411, L1
Michael S., Durisen R. H., Boley A. C., 2011, ApJ, 737, L42
Mizuno H., 1980, Prog. Theor. Phys., 64, 544
Moorhead A. V., Adams F. C., 2008, Icarus, 193, 475
Mordasini C., Alibert Y., Benz W., Klahr H., Henning T., 2012, A&A, 541, A97
Nagasawa M., Ida S., 2011, ApJ, 742, 72
Nayakshin S., 2010a, MNRAS, 408, L36
Nayakshin S., 2010b, MNRAS, 408, 2381
Nayakshin S., 2011a, MNRAS, 410, L1
Nayakshin S., 2011b, MNRAS, 413, 1462

Nayakshin S., 2011c, MNRAS, 416, 2974
Nayakshin S., Cha S.-H., 2012, MNRAS, 423, 2104
Nayakshin S., Lodato G., 2012, MNRAS, 426, 70
Nettelmann N., 2011, Astrophys. Space Sci., 336, 47
Ogilvie G. I., Lubow S. H., 2003, ApJ, 587, 398
Owen J. E., Ercolano B., Clarke C. J., Alexander R. D., 2010, MNRAS, 401, 1415
Owen J. E., Ercolano B., Clarke C. J., 2011, MNRAS, 412, 13
Paardekooper S.-J., 2012, MNRAS, 421, 3286
Paczynski B., 1978, Acta Astron., 28, 91
Podlewska-Gaca E., Papaloizou J. C. B., Szuszkiewicz E., 2012, MNRAS, 421, 1736
Pollack J., 1996, Icarus, 124, 62
Pringle J. E., 1981, ARA&A, 19, 137
Rafikov R., 2005, ApJ, 621, 69
Rees M. J., 1976, MNRAS, 176, 483
Rice W. K. M., Armitage P. J., 2009, MNRAS, 396, 2228
Rice W. K. M., Lodato G., Pringle J. E., Armitage P. J., Bonnell I. A., 2004, MNRAS, 355, 543
Rice W. K. M., Lodato G., Armitage P. J., 2005, MNRAS, 364, L56
Rice W. K. M., Mayo J. H., Armitage P. J., 2010, MNRAS, 402, 1740
Rice W. K. M., Armitage P. J., Mamatsashvili G. R., Lodato G., Clarke C. J., 2011, MNRAS, 418, 1356
Rice W. K. M., Forgan D. H., Armitage P. J., 2012, MNRAS, 420, 1640
Rogers P. D., Wadsley J., 2012, MNRAS, 423, 1896
Shabram M., Boley A. C., 2013, ApJ, 767, 63
Shakura N. I., Sunyaev R. A., 1973, A&A, 24, 337
Stamatellos D., 2013, preprint (arXiv:1302.3955)
Stamatellos D., Whitworth A. P., 2008, A&A, 480, 879
Stamatellos D., Whitworth A. P., 2009, MNRAS, 392, 413
Stamatellos D., Whitworth A. P., Hubber D. A., 2012, MNRAS, 427, 1182
Toomre A., 1964, ApJ, 139, 1217
Vorobyov E. I., Basu S., 2005, ApJ, 633, L137
Vorobyov E. I., Basu S., 2006, ApJ, 650, 956
Vorobyov E. I., Basu S., 2010, ApJ, 714, L133
Weidenschilling S. J., 1977, MNRAS, 180, 57
Whipple F. L., 1973, in Hemenway C., Millman P., Cook A., eds, IAU Colloq. 13: Radial Pressure in the Solar Nebula as Affecting the Motions of Planetesimals. NASA SP, 319, 355
Whitworth A. P., Stamatellos D., 2006, A&A, 458, 817
Windmark F., Birnstiel T., Güttler C., Blum J., Dullemond C. P., Henning T., 2012, A&A, 540, A73
Zhu Z., Hartmann L., Gammie C., McKinney J. C., 2009, ApJ, 701, 620
Zhu Z., Hartmann L., Nelson R. P., Gammie C. F., 2012, ApJ, 746, 110

This paper has been typeset from a TEX/LATEX file prepared by the author.